

# Octahedral Bipyridine and Bipyrimidine Dioxomolybdenum(VI) Complexes: Characterization, Application in Catalytic Epoxidation, and Density Functional Mechanistic Study

Fritz E. Kühn,<sup>\*,[a]</sup> Michelle Groarke,<sup>[a]</sup> Éva Bencze,<sup>[a]</sup> Eberhardt Herdtweck,<sup>[a]</sup> Angela Prazeres,<sup>[b]</sup> Ana M. Santos,<sup>[a, b]</sup> Maria J. Calhorda,<sup>[b, c]</sup> Carlos C. Romão,<sup>\*,[b]</sup> Isabel S. Gonçalves,<sup>[b, d]</sup> André D. Lopes,<sup>[e]</sup> and Martyn Pillinger<sup>[d]</sup>

**Abstract:** Complexes of the general formula  $[\text{MoO}_2\text{X}_2\text{L}_2]$  ( $\text{X} = \text{Cl}, \text{Br}, \text{Me}$ ;  $\text{L}_2 = \text{bipy}, \text{bpym}$ ) have been prepared and fully characterized, including X-ray crystallographic investigations of all six compounds. Additionally, the highly soluble complex  $[\text{MoO}_2\text{Cl}_2(4,4'\text{-bis}(\text{hexyl})\text{-}2,2'\text{-bipyridine})]$  has been synthesized. The reaction of the complexes with *tert*-butyl hydroperoxide (TBHP) is an equilibrium reaction, and leads to  $\text{Mo}^{\text{VI}} \eta^1\text{-alkylperoxo}$  complexes that se-

lectively catalyze the epoxidation of olefins. Neither the  $\text{Mo}-\text{X}$  bonds nor the  $\text{Mo}-\text{N}$  bonds are cleaved during this reaction. These experimental results are supported by theoretical calculations, which show that the attack of TBHP at

the Mo center through the X-O-N face is energetically favored and the TBHP hydrogen atom is transferred to a terminal oxygen of the  $\text{Mo}=\text{O}$  moiety. After the attack of the olefin on the Mo-bound peroxo oxygen atom, epoxide and *tert*-butyl alcohol are formed. The latter compound acts as a competitive inhibitor for the TBHP attack, and leads to a significant reduction in the catalytic activity with increasing reaction time.

**Keywords:** density functional calculations • homogeneous catalysis • molybdenum • N ligands • reaction mechanisms

## Introduction

Dioxomolybdenum(VI) complexes are important catalysts or catalyst precursors for oxygen-atom transfer reactions in chemical and biological systems.<sup>[1]</sup> Polymeric compounds of the composition  $[\text{MoO}_2\text{X}_2]$  have been known for more than 100 years.<sup>[2a]</sup> With Lewis bases, such as 2,2'-bipyridine, and with donor solvents, such as acetonitrile, adducts of the composition  $[\text{MoO}_2\text{X}_2\text{L}_2]^{[\neq]}$  are formed.<sup>[2b,c]</sup> The first X-ray crystal structure of a  $[\text{MoO}_2\text{X}_2\text{L}_2]$ -type complex was reported in 1966.<sup>[2d]</sup> The  $[\text{MoO}_2\text{X}_2\text{L}_2]$  complexes are monomeric and present a distorted octahedral geometry, with the oxo ligands *cis* to each other in order to maximize backdonation into the empty  $t_{2g}$  set orbitals.<sup>[2e]</sup>

Particular interest in  $\text{Mo}^{\text{VI}}\text{-oxo}$  complexes arose in the late 1960's when ARCO and Halcon presented patents on the olefin epoxidation catalyzed by  $\text{Mo}^{\text{VI}}$  compounds in a homogeneous phase.<sup>[2f,g]</sup> In the following years different mechanisms were suggested to explain the reactivity of these complexes. The debate as to which of the two main proposed mechanisms is more accurate, the one favored by Mimoun et al.<sup>[2h]</sup> or the one suggested by Sharpless et al.<sup>[2i]</sup> has not been settled to date, despite the fact that several theoretical and


[a] Priv. Doz. Dr. F. E. Kühn, Dr. M. Groarke, Dr. É. Bencze, Dr. E. Herdtweck, Dr. A. M. Santos  
Anorganisch-chemisches Institut  
der Technischen Universität München  
Lichtenbergstr. 4, 85747 Garching b. München (Germany).  
E-mail: fritz.kuehn@ch.tum.de

[b] Prof. Dr. C. C. Romão, Dipl.-Chem. A. Prazeres, Dr. A. M. Santos, Prof. Dr. M. J. Calhorda, Prof. Dr. I. S. Gonçalves  
Instituto de Tecnologia Química e Biológica  
da Universidade Nova de Lisboa  
Quinta do Marquês, EAN, Apt. 127, 2781-901 Oeiras (Portugal)  
E-mail: mjc@itqb.unl.pt, ccr@itqb.unl.pt

[c] Prof. Dr. M. J. Calhorda  
Departamento de Química, Faculdade de Ciências  
Universidade de Lisboa, 1749-016 Lisboa (Portugal)

[d] Prof. Dr. I. S. Gonçalves, Dr. M. Pillinger  
Departamento de Química, Universidade de Aveiro  
Campus de Santiago, 3810-193 Aveiro (Portugal)

[e] Prof. Dr. A. D. Lopes  
Faculdade de Ciências e Tecnologia  
Área Departamental de Química  
Universidade do Algarve, Campus de Gambelas  
8000-062 Faro (Portugal)

 Supporting information for this article is available on the WWW under <http://www.wiley-vch.de/home/chemistry/> or from the author. ORTEP-style drawings of all structures determined in this work and figures to illustrate the observed distortions in the structures are provided. An additional figure to illustrate the powder X-ray experiments is also available.

[≠] Throughout this manuscript  $\text{L}_2$  denotes either two monodentate ligands or one bidentate ligand.

mechanistic studies have been presented.<sup>[2j]</sup> It has been generally agreed, however, that formation of a Mo<sup>VI</sup> alkyl peroxide occurs followed by transfer of the distal oxygen atom of the alkyl peroxide rather than an oxo ligand.<sup>[2k]</sup> The industrial ARCO–Halcon process employs *tert*-butyl hydroperoxide (TBHP) as an oxidizing agent. Despite the fact that H<sub>2</sub>O<sub>2</sub> is a more environmentally friendly oxidant (the only byproduct formed is H<sub>2</sub>O), TBHP has other advantages that still make it the preferred oxidizing agent in industrial processes.<sup>[2l]</sup> However, several attempts have been made to employ H<sub>2</sub>O<sub>2</sub> as the oxidizing system for olefin epoxidation, most notably based on [CH<sub>3</sub>ReO<sub>3</sub>] by Herrmann et al.<sup>[2m]</sup> and on modified Mo<sup>VI</sup> systems by Sundermeyer et al.<sup>[2n]</sup> In the early 1980's, Mimoun et al. assumed that the [MoO<sub>2</sub>X<sub>2</sub>L<sub>2</sub>] complexes are transformed into [Mo(O<sub>2</sub>)<sub>2</sub>OL<sub>2</sub>] in the presence of excess H<sub>2</sub>O<sub>2</sub>.<sup>[2o]</sup> The reaction of [MoO<sub>2</sub>X<sub>2</sub>L<sub>2</sub>] with excess TBHP, however, remained unclear. We have recently published a series of papers which show that complexes of the type [MoO<sub>2</sub>X<sub>2</sub>L<sub>2</sub>] are excellent catalyst precursors for the olefin epoxidation in the presence of TBHP.<sup>[3]</sup> The question of the catalytically active species and a possible reaction mechanism, however, remained unanswered. In this paper we present a systematic examination of selected complexes of the type [MoO<sub>2</sub>X<sub>2</sub>L<sub>2</sub>] (X = Cl, Br, Me; L<sub>2</sub> = 2,2'-bipyridine, 2,2'-bipyrimidine, 4,4'-bis(*n*-hexyl)-2,2'-bipyridine) with respect to their structures, spectroscopic data, and catalytic performance. Some of the older literature data are shown to be inaccurate or even incorrect. Additionally, we present a suggestion for the reaction mechanism based both on experimental data and on theoretical calculations, and demonstrate that during the course of catalysis neither the Mo–X bond nor the Mo–N bonds are disrupted, as has been previously speculated.

## Results and Discussion

### Preparation and characterization of the dioxomolybdenum(vi) complexes

**Synthesis:** The oxo–molybdenum complexes used in this work, [MoO<sub>2</sub>X<sub>2</sub>L<sub>2</sub>] (X = Br, Cl, Me; L<sub>2</sub> = 2,2'-bipyridine (bipy), 2,2'-bipyrimidine (bpym), 4,4'-bis(*n*-hexyl)-2,2'-bipyridine), were prepared by the route previously described for related Mo<sup>VI</sup> dioxo complexes.<sup>[3a,c,4]</sup> The halogeno products **1**, **2**, **4**, **5**, and **7** were obtained in good yields within a few minutes. The product complexes **1**, **2**, **4**, and **5** precipitate from the reaction mixture. Compound **7** only precipitates from a reduced solvent volume after addition of *n*-hexane. Treatment of [MoO<sub>2</sub>X<sub>2</sub>L<sub>2</sub>] (L<sub>2</sub> = bipy, bpym) with Grignard reagents at low temperatures yields the methyl complexes **3** and **6**. All of the compounds are stable under laboratory atmosphere and can be readily handled in air.

**NMR spectroscopy:** The <sup>95</sup>Mo NMR spectra of the complexes **1–7** reflect the inductive effects of the substituents X and the pK<sub>a</sub> values of the ligands L. The X substituents show an inverse ligand dependence, which has been confirmed by theoretical calculations and is known from related compounds

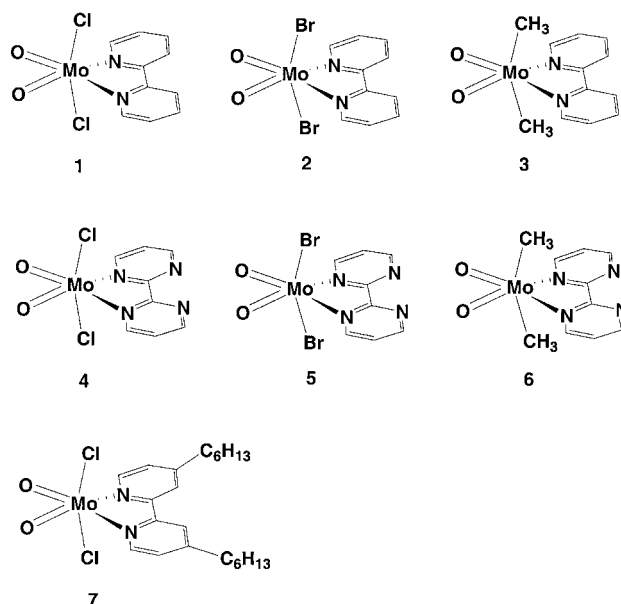


(Table 1).<sup>[3,5]</sup> The differences in the <sup>95</sup>Mo shift between the bipyrimidine and the bipyridine ligand is comparatively small, only a few ppm in each case. The difference in the chemical shift between Cl and Br is  $\approx 50$  ppm, and between the Br and the CH<sub>3</sub> ligands it is nearly 200 ppm. Complexes of the composition [MoO<sub>2</sub>Cl<sub>2</sub>L<sub>2</sub>] generally display their <sup>95</sup>Mo NMR signals at  $\delta(^{95}\text{Mo}) = 160\text{--}220$ , whereas the bromine derivatives show their <sup>95</sup>Mo signals between  $\delta = 170$  and 280; the shift differences between bromo and chloro derivatives is usually  $\approx 30\text{--}60$  ppm.<sup>[3b]</sup> The methyl complexes of the general formula [MoO<sub>2</sub>(CH<sub>3</sub>)<sub>2</sub>L<sub>2</sub>] described in the literature display their Mo central atom at chemical shifts between  $\delta = 370$  and 520. Methyl complexes with *N*-bidentate heterocyclic aromatic ligands display their signals in the high-field region of this range between  $\delta = 370$  and 450.<sup>[3d]</sup>

Table 1. <sup>95</sup>Mo NMR and <sup>17</sup>O NMR shifts of [MoR<sub>2</sub>O<sub>2</sub>L<sub>2</sub>] complexes (R = CH<sub>3</sub>, Br, Cl).

Com- pound	$\delta(^{95}\text{Mo})$	$\delta(^{17}\text{O})$	$f(\text{Mo}=\text{O})$ [mdyn Å <sup>-1</sup> ]	TOF [h <sup>-1</sup> ]
<b>1</b>	182 (DMSO)	[a]	6.73	25
<b>2</b>	232 (DMSO)	[a]	6.70	10
<b>3</b>	425 (NCMe)	[a]	6.65	8
<b>4</b>	175 (NCMe)	997 (NCMe)	6.82	50
<b>5</b>	228 (NCMe)	996 (NCMe)	6.79	21
<b>6</b>	422 (CH <sub>2</sub> Cl <sub>2</sub> )	843 (CH <sub>2</sub> Cl <sub>2</sub> )	6.70	16
<b>7</b>	190 (CDCl <sub>3</sub> )	995 (CDCl <sub>3</sub> )	6.68	80

[a] Not determined.

On account of the very poor solubility of the bipyridine complexes, the <sup>17</sup>O NMR spectra of complexes **1–3** were not of sufficient quality, in spite of <sup>17</sup>O labeling of the compounds. In the case of the bipyrimidine compounds, however, spectra were obtained. The chemical shift found for compound **4** is  $\delta(^{17}\text{O}) = 997$ . While the <sup>17</sup>O chemical shift of the bromo derivative is identical within the error range ( $\delta(^{17}\text{O}) = 996$ ), the shift difference to the methyl derivative is  $\approx 150$  ppm ( $\delta(^{17}\text{O}) = 843$ ). Compound **7** is significantly more soluble than

the unsubstituted bipy congener **1** and has a  $^{17}\text{O}$  NMR signal at  $\delta = 995$ . The chemical shifts of the equatorial oxygen atoms of all these complexes are in the expected range. The few  $^{17}\text{O}$  NMR chemical shifts published for complexes of the formula  $[\text{MoO}_2\text{X}_2\text{L}_2]$  are in the range of  $\delta = 925\text{--}970$ . However, the shift difference between chloro and bromo derivatives is more pronounced in the compounds which have been previously examined ( $\approx 20\text{--}40$  ppm).<sup>[5b]</sup> Although literature data on methyl complexes of the formula  $[\text{MoO}_2\text{X}_2\text{L}_2]$  were not available, the observed shift to higher field is expected because of their lower Lewis acidity.

**IR/Raman spectroscopy:** The experimental results (see also Tables 1 and 2) obtained for the chlorine and bromine derivatives **1**, **2**, **4**, **5**, and **7** show that the halide substituents do not influence the stretching vibrations of the equatorial  $\text{MoO}_2\text{N}_2$  plane to a very significant extent. The  $\text{M}=\text{O}$  and the  $\text{M}-\text{X}$  ( $\text{X} = \text{Cl}, \text{Br}, \text{Me}$ ) vibrations of the bpym complexes are always shifted to higher wavenumbers. This is indicative of stronger metal–ligand interactions. Additionally, this trend is reflected in the calculated force constants (see Table 1). These observations are in accord with the  $\text{p}K_{\text{a}}$  values of bipy (4.3) and bpym (0.6). The weaker base, bpym, donates less electron density to the electron-deficient metal center. Accordingly, more electron density is shifted from the other ligands thereby strengthening the ligand–metal bonds. A comparison of the observed vibrational spectroscopic values for the complexes **3** and **6** (see Table 2) indicates that the replacement of a halide by a methyl group considerably weakens the equatorial metal–ligand bonds. The observed stretching vibrations as well as the calculated force constants (see Table 1) show for both complex series, **1–3** and **4–6**, that the  $\text{Mo}-\text{O}$  bond strength increases in the order  $\text{CH}_3 < \text{Br} < \text{Cl}$ , in accordance with the inductive effects of these three ligands.

**X-ray crystallography—perspective from a valence-shell electron-pair repulsion model:** The solid-state crystal structures of complexes **1–6** were obtained by single-crystal X-ray experi-

ments. Key bond lengths and angles are listed in Table 3. Fenn<sup>[6]</sup> first reported the molecular structure of complex **2** in 1969 to be a strongly distorted octahedron around the molybdenum center. Both the  $\text{Mo}-\text{Br}$  (2.781(3)–2.461(3) Å) and the  $\text{Mo}=\text{O}$  (1.826(18)–1.643(17) Å) bond lengths show significant differences. For obvious reasons, such as 1) incomplete photographically collected data ( $h,k,0-6$ ), 2) use of copper radiation ( $\mu = 16.743\text{ mm}^{-1}$ ), and 3) no absorption correction applied, we assign this doubtful observation to be caused by a fragmentary data set with severe systematic errors and to the visually integrated intensities. The molecular structure of **2** was therefore redetermined. Detailed X-ray crystallographic experiments of **3**, **5**, and **6** are published elsewhere.<sup>[4a, 3a,d]</sup> All six compounds are monomeric and belong to the general core geometry of type  $[\text{MO}_2\text{N}_2\text{X}_2]$  ( $\text{M} = \text{transition metal}, \text{X} = \text{any atom}$ ) (Figure 1). In detail, compounds **1–6** belong to the representative **B**-type (see ref. [3a]). The X atoms are located in the apical position of a more or less distorted octahedron around the metal center. The  $\text{X}-\text{Mo}-\text{X}$  angles range from  $148.0(1)^\circ$  to  $159.64(2)^\circ$  with a mean value of  $155.3^\circ$ , and the  $\text{O}=\text{Mo}=\text{O}$  angles range from  $106.3(1)^\circ$  to  $110.26(9)^\circ$  with a mean value of  $108.0^\circ$ . The oxygen atoms are in *cis* positions and define the equatorial plane together with the transition metal and two nitrogen atoms of the Lewis base ligand. However, the transition metal is off-center and shifted away from the nitrogen atoms towards the midpoint of the two oxygen atoms.

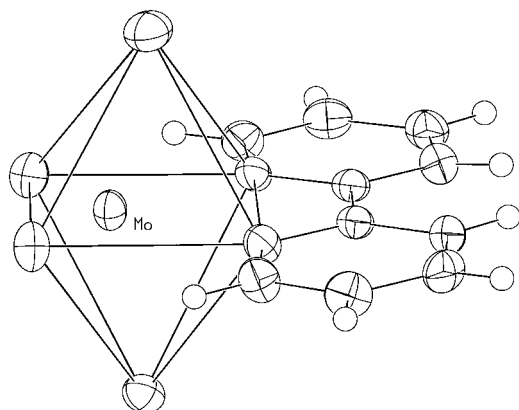
**Approach from a pure solid-state ionic model:** Based on the core geometry of the  $[\text{MO}_2\text{N}_2\text{X}_2]$  complexes, an unrestricted search in the Cambridge Structural Database revealed 8007 hits.<sup>[7a]</sup> The very high hit rate demonstrates that this ligand combination is very common and of basic scientific interest. The second search that was restricted to **B**-type core geometry and  $\text{M} = \text{Mo}$  gave 20 hits.<sup>[7b]</sup> The ranges of bond lengths and angles spanned by these 20 compounds encompass the crystallographic data of compounds **1–6**, even the

Table 2. Selected IR and Raman stretching frequencies of the complexes **1–7**.

	<b>1</b>		<b>2</b>		<b>3</b>		<b>7</b>	
	IR	Raman	IR	Raman	IR	Raman	IR	Raman
$\text{MoO}_2$ sym. str.	936 s	931 vvs	933 s	928 s	930 s	924 vs	938 vs	940 vs
$\text{MoO}_2$ asym. str.	904 vs	906 s	902 vs	904 s	897 vs	897 m	912 vs	916 m
$\text{MoC}_2$ asym. str.	–	–	–	–	493 s	490 vvw	–	–
$\text{MoC}_2$ sym. str.	–	–	–	–	466 w	468 s	–	–
$\text{MoX}_2$ asym. str.	338 vs	341 w	253 s	255 m	–	–	344 s	354 w
$\text{MoX}_2$ sym. str.	243 m	242 s	–	134 sh	–	–	236 s	–
$\text{MoN}_2$ sym. str.	207 w	214 vs	217 m	219 s	227 m	224 s	203 m	215 s
$\text{MoN}_2$ asym. str.	192 m	193 w	207 m	207 s	195 w	–	190 m	–
	<b>4</b>		<b>5</b>		<b>6</b>			
	IR	Raman	IR	Raman	IR	Raman		
$\text{MoO}_2$ sym. str.	943 s	940 vvs	941 s	938vs	936 s	928 vvs		
$\text{MoO}_2$ asym. str.	910 vs	907 s	909 s	907 m	902 vs	902 sm		
$\text{MoC}_2$ asym. str.	–	–	–	–	503 m	505 sm		
$\text{MoC}_2$ sym. str.	–	–	–	–	477 w	477 vs		
$\text{MoX}_2$ asym. str.	355 s	357 w	258 s	255 w	–	–		
$\text{MoX}_2$ sym. str.	240 m	238 m	–	133 vw	–	–		
$\text{MoN}_2$ sym. str.	220 w	224 vs	219 m	212 sh	231 m	229 s		
$\text{MoN}_2$ asym. str.	210 w	207 m	210 m	198 s	216 w	–		

Table 3. Selected interatomic distances [ $\text{\AA}$ ] and angles [ $^\circ$ ] for compounds  $[\text{MoX}_2\text{O}_2\text{L}_2]$ .  $\text{L}_2 = \text{bipy}$ : (X = Cl (**1**), Br (**2**),  $\text{CH}_3$  (**3**));  $\text{L}_2 = \text{bpym}$ : (X = Cl (**4**), Br (**5**),  $\text{CH}_3$  (**6**)).

	<b>1</b>	<b>2</b>	<b>3</b> (Ref. [4a])	<b>4</b>	<b>5</b> (Ref. [3a])	<b>6</b> (Ref. [3d])
Mo–X1	2.366(1)	2.5105(7)	2.189	2.3678(6)	2.5330(5)	2.187(3)
Mo–X2	2.3769(9)	2.5245(6)	2.194	2.3456(6)	2.5342(5)	2.190(2)
Mo–O1	1.699(2)	1.728(3)	1.707	1.692(2)	1.693(3)	1.699(2)
Mo–O2	1.697(3)	1.711(4)	1.708	1.699(2)	1.697(2)	1.717(2)
Mo–N12	2.298(3)	2.293(5)	2.314	2.355(2)	2.326(3)	2.364(2)
Mo–N22	2.323(2)	2.317(4)	2.346	2.332(2)	2.316(2)	2.336(2)
O...O	2.717(4)	2.762(5)	2.801	2.734(3)	2.725(4)	2.803(2)
X1–Mo–X2	158.52(4)	158.96(2)	149.02	159.64(2)	157.67(2)	148.0(1)
X1–Mo–O1	96.12(8)	95.7(1)	98.31	95.45(6)	95.95(9)	101.3(1)
X1–Mo–O2	97.82(8)	97.6(1)	99.88	97.08(5)	96.08(9)	97.84(9)
X1–Mo–N12	80.61(6)	80.8(1)	76.55	81.86(4)	81.77(8)	79.75(9)
X1–Mo–N22	81.89(6)	81.98(9)	77.95	80.61(4)	81.94(6)	74.25(9)
X2–Mo–O1	95.54(7)	95.2(1)	97.60	96.35(6)	97.45(8)	99.5(1)
X2–Mo–O2	96.13(8)	96.4(1)	99.30	95.11(5)	96.97(8)	97.43(9)
X2–Mo–N12	80.65(6)	80.5(1)	76.31	80.91(4)	79.87(8)	76.89(9)
X2–Mo–N22	81.78(6)	82.50(8)	78.39	83.09(4)	79.66(6)	76.7(1)
O1–Mo–O2	106.3(1)	106.9(2)	110.21	107.49(8)	107.0(1)	110.26(9)
O1–Mo–N12	93.9(1)	93.8(2)	92.65	93.50(7)	92.6(1)	88.13(9)
O1–Mo–N22	163.4(1)	163.4(2)	161.04	162.20(7)	161.4(1)	155.52(9)
O2–Mo–N12	159.7(1)	159.3(1)	157.13	158.97(7)	160.4(1)	161.51(8)
O2–Mo–N22	90.3(1)	89.8(2)	88.74	90.26(7)	91.6(1)	94.23(8)
N12–Mo–N22	69.45(9)	69.6(2)	68.39	68.80(6)	68.82(9)	67.41(7)

Figure 1. Schematic ORTEP<sup>[30b]</sup> drawing of the molecular structure of **2** showing the dislocation of the central transition metal.

mean values are identical (Mo=O: from 1.680  $\text{\AA}$  to 1.740  $\text{\AA}$ , mean 1.702  $\text{\AA}$ ; X–Mo–X: from 145.5° to 160.8°, mean 154.7°; O=Mo=O: from 104.4° to 113.1°, mean 107.9°). A more unrestricted third search that allowed the equatorial and axial ligands to be linked revealed 138 hits,<sup>[7c]</sup> including the transition metals V<sup>V</sup> (e.g.,  $[\text{VO}_2(\text{tpen})]\text{Cl} \cdot \text{H}_2\text{O}$ ,<sup>[8j]</sup>), Mo<sup>VI</sup>, W<sup>VI</sup> (e.g.,  $[\text{WO}_2\text{L}]$ ,<sup>[9]</sup>), and Re<sup>VII</sup> (e.g.,  $[\text{ReO}_3(\text{Br})(t\text{Bu-bipy})]$ ,<sup>[10]</sup>). The ranges of the observed bond lengths and angles are somewhat larger than those obtained in the second search (M=O: from 1.615 to 1.757  $\text{\AA}$ , mean value 1.701  $\text{\AA}$ ; X–M–X: from 143.1° to 171.7°, mean value 154.5°; O=M=O: from 102.2° to 115.1°, mean value 107.0°). However, the mean values appear to be invariant. Such an excellent agreement in terms of bond lengths and angles of a wide variety of ligands X and transition metals point to a geometrically invariable and rigid ligand sphere  $\{\text{O}_2\text{N}_2\text{X}_2\}$ . When the midpoint of the equatorial  $\text{O}_2\text{N}_2$ -plane ( $\text{C}_g$ ) is defined to be the center of the  $\{\text{O}_2\text{N}_2\text{X}_2\}$  octahedron, and bond lengths and angles around  $\text{C}_g$

are recalculated, the  $\{\text{O}_2\text{N}_2\text{X}_2\}$  octahedra are elongated, but still regular (Table 4, Figure 1).<sup>[11–13]</sup>

As far as is known from the literature and from our own experiments, the free ligands biphenyl,<sup>[14]</sup> bipyridyl,<sup>[15]</sup> and bipyrimidine<sup>[16]</sup> are centrosymmetric and planar in the solid state. The observed slightly twisted and tilted distortions of the  $N,N$  ligands in compounds **1–6** are not unexpected.

**X-ray powder diffraction:** Powder X-ray diffraction (XRD) patterns were recorded for the synthesized dioxomolybdenum(vi) complexes **1–6** and compared with simulated patterns calculated from the single-crystal structure data reported in this paper for **1**, **2**, **4–6**, and reference [4a] for **3**. In each case there was a good match between the experimental and simulated patterns, indicating a high degree of purity and crystallinity for the as-synthesized complexes.

### Catalytic and mechanistic studies of cyclooctene epoxidation

**Catalytic Studies:** Compounds **1–7** were tested as catalysts in cyclooctene epoxidation reactions with TBHP as the oxidizing agent. The reactions were performed at 55 °C in *n*-decane. The ratio catalyst/substrate/oxidizing agent was 1:100:200. More details are given in the Experimental Section. Complexes **1–7** are not very active catalysts. The turnover frequencies (TOFs) determined for these complexes are given in Table 1. In general, the TOFs of the bipyrimidine derivatives **4–6** are approximately twice as high as those of the bipyridine complexes. Compound **7** is the most active catalyst among the compounds examined in this work. The chlorine derivatives show higher TOFs than the bromine complexes, and the bromine compounds are slightly more active than the methyl compounds. These observations evidently reflect the inductive effects of the ligands L and X. The TOFs seem to be much more sensitive to changes in the electron density at the metal center than most of the spectroscopic methods we applied,

Table 4. Idealized core geometry (bond lengths [Å] and angles [°]) for B-type compounds [MX<sub>2</sub>O<sub>2</sub>N<sub>2</sub>] around the center C<sub>g</sub>.

	1	2	3 (Ref. [4a])	4	5 (Ref. [3a])	6 (Ref. [3d])	V <sup>V</sup> (Ref. [8])	W <sup>VI</sup> (Ref. [9])	Re <sup>VII</sup> (Ref. [10])
C <sub>g</sub> -X1	2.334	2.475	2.118	2.327	2.498	2.120	2.101	1.882	2.408
C <sub>g</sub> -X2	2.327	2.478	2.115	2.313	2.474	2.100	2.101	1.916	1.901
C <sub>g</sub> -O1	2.017	2.040	2.043	2.020	2.001	1.982	1.918	2.053	1.971
C <sub>g</sub> -O2	1.969	1.977	1.992	1.992	1.995	2.072	1.918	1.979	1.965
C <sub>g</sub> -N12	1.965	1.964	1.954	1.997	1.971	1.959	2.010	1.987	1.903
C <sub>g</sub> -N22	1.964	1.963	1.957	1.957	1.956	1.965	2.010	2.022	1.922
O...O	2.717	2.762	2.801	2.734	2.725	2.803	2.613	2.776	2.764
X1-C <sub>g</sub> -X2	176.92	176.25	172.81	177.16	178.25	171.26	173.12	175.62	178.47
X1-C <sub>g</sub> -O1	88.95	89.19	90.85	88.38	89.61	94.85	88.94	88.43	89.89
X1-C <sub>g</sub> -O2	91.53	91.97	93.68	90.61	89.92	89.80	86.02	90.79	89.14
X1-C <sub>g</sub> -N12	88.70	88.48	86.47	91.05	90.09	91.43	81.58	87.19	90.76
X1-C <sub>g</sub> -N22	90.85	90.39	88.89	89.97	90.39	83.88	103.32	93.60	90.24
X2-C <sub>g</sub> -O1	88.98	89.10	90.48	88.84	91.60	93.88	86.02	87.64	88.93
X2-C <sub>g</sub> -O2	90.60	91.27	93.42	88.62	91.43	90.10	88.94	90.94	89.87
X2-C <sub>g</sub> -N12	89.23	88.36	86.38	89.79	88.54	88.55	103.32	91.15	90.26
X2-C <sub>g</sub> -N22	91.21	91.30	89.62	92.81	88.39	87.43	81.58	90.34	90.97
O1-C <sub>g</sub> -O2	85.96	86.88	87.93	85.92	86.00	87.45	85.89	86.99	89.21
O1-C <sub>g</sub> -N12	95.61	95.39	94.64	95.91	95.35	93.32	92.66	93.95	92.32
O1-C <sub>g</sub> -N22	179.67	179.32	178.75	178.35	179.18	176.39	167.54	177.97	178.12
O2-C <sub>g</sub> -N12	178.42	177.69	177.43	177.56	178.65	178.49	167.54	177.74	178.46
O2-C <sub>g</sub> -N22	94.30	93.67	93.31	94.13	94.82	95.92	92.66	92.88	92.67
N12-C <sub>g</sub> -N22	84.13	84.07	84.12	84.09	83.83	83.35	91.37	86.26	85.80

since the differences in activity are rather pronounced. It is astonishing, however, that the activity differences of the chlorine and the bromine compounds are very pronounced, while the activities of the bromo and the methyl complexes are more similar. From the spectroscopic data (IR/Raman and NMR) the opposite should be expected. As the steric bulk of the ligands L (bipyridine and bipyrimidine) is rather similar, then electronic factors must be responsible for the activity differences in these cases. In the case of the Cl and the Br/CH<sub>3</sub> derivatives, steric factors may play an additional role and thus partially account for the activity differences. Comparing the activities determined in this work with literature values of other complexes of the formula [MoO<sub>2</sub>X<sub>2</sub>L<sub>2</sub>], compounds **1–7** are rather sluggish catalysts of low general activity.<sup>[3]</sup> With complexes of the type [MoO<sub>2</sub>X<sub>2</sub>L<sub>2</sub>], TOFs of up to ≈600 mol mol<sup>-1</sup> h<sup>-1</sup> have been reached, while Br and Me derivatives are reported to reach TOFs of not more than 200 mol mol<sup>-1</sup> h<sup>-1</sup>. It should be noted in this context that the Re<sup>VII</sup> complexes [ReO<sub>3</sub>(CH<sub>3</sub>)(bipy)] (TOF at 55 °C ≈200 mol mol<sup>-1</sup> h<sup>-1</sup>) and [ReO<sub>3</sub>(CH<sub>3</sub>)(bpym)] (TOF at 55 °C ≈400 mol mol<sup>-1</sup> h<sup>-1</sup>) are reported to be quite good epoxidation catalysts.<sup>[17, 18]</sup> Their activity surpasses that of all Mo<sup>VI</sup>-bipy and Mo<sup>VI</sup>-bpym complexes examined here to a significant extent. The higher catalytic activity of the [ReO<sub>3</sub>(CH<sub>3</sub>)(bpym)] complex is very probably caused by the higher Lewis acidity of the metal center. General statements such as this have to be regarded with caution, however, since the catalytic mechanisms are quite different and different oxidizing agents have to be applied in the Re<sup>VII</sup> case (H<sub>2</sub>O<sub>2</sub>) and in the Mo<sup>VI</sup> case (TBHP).<sup>[17]</sup>

The trends observed in the complexes described in this work are exemplary for all compounds of this type: the chlorine derivatives are more active as epoxidation catalysts than the bromine complexes, which are usually only slightly more active than the methyl complexes. More important than the axial ligands X are the equatorial donor ligands L, which

can vary the catalytic activity in a broad range. The complexes described in this work are on the lower end of the activity level. Only very bulky ligands L, for example bidentate phenanthroline derivatives, display an even lower catalytic activity.<sup>[34]</sup>

Nevertheless, all of the [MoO<sub>2</sub>X<sub>2</sub>L<sub>2</sub>] catalysts show the same type of reaction curve in the olefin epoxidation with TBHP. After a comparatively rapid increase in the product yield in the earlier stages, the reaction slows down considerably during the course of the catalytic run. Several factors can be responsible for this behavior. Together with the normal decrease of activity as a result of the consumption of both substrate and oxidizing agent, catalyst decomposition or hindrance of the reaction by one of the reaction products can play an important role.

The following reactions were performed with compound **7** as an exemplary catalyst precursor. We first examined the influence of the byproduct *tert*-butyl alcohol on the reaction. It was found that when 10% of the alcohol was added at the start of the reaction, a noticeable decrease in yield in comparison to the reaction without alcohol addition is observed. When the alcohol is added after 25 min, there is still a pronounced effect. Evidently, the alcohol competes for coordination to the Mo center and therefore slows down the reaction rate.

A further set of experiments was performed to explore the stability of the catalyst. After 24 h reaction time, when the product yield reached ≈75%, more substrate was added to the reaction mixture. The catalyst was still active, albeit somewhat slower in catalyzing the reaction. This is most probably caused by the large excess of *tert*-butyl alcohol present in the reaction mixture which hinders the reaction process. We also tried to isolate the catalyst after one catalytic run. However, the compound we received was not the catalyst itself, but compound **7**, the catalyst precursor (an explanation for this observation is given in the next section). The reuse of

this isolated compound in a catalytic cycle led to an activity that was the same as in the first run, within the range of experimental error. Thus, it is reasonable to assume that the “leveling off” of epoxide yields with  $[\text{MoO}_2\text{Cl}_2\text{L}_2]$  complexes as catalysts results from inhibition by *tert*-butyl alcohol in the reaction mixture and not from catalyst decomposition.

Further evidence for the latter assumption is that we never observed the formation of  $\text{CH}_4$ ,  $\text{C}_2\text{H}_6$ , or  $\text{CH}_3\text{OH}$  when compounds **3** and **6** were used as catalyst precursors for a catalytic run at  $55^\circ\text{C}$ . Small amounts of  $\text{CH}_4$  were only formed at a reaction temperature of  $90^\circ\text{C}$ . It can be seen from the GC/MS results that at temperatures above  $75^\circ\text{C}$  the increase of the product yield is no longer linear, so that catalyst decomposition may play a role at those temperatures, especially in the case of the methyl derivative **6**.

**Spectroscopic studies:** It is well known that adducts of methyltrioxorhenium (MTO) with Lewis bases are very efficient and selective epoxidation catalysts although they readily exchange their Lewis-base ligands.<sup>[19a]</sup> Therefore, we examined whether the  $\text{Mo}^{\text{VI}}$  complexes studied in this work display a similar behavior. On the contrary, the reaction of a solution of complex **7** with two equivalents of 2,2'-bipyridine did not lead to any observable ligand exchange even after two days. Furthermore, the oxygen atoms of the molybdenum complexes are also found not to exchange under catalysis conditions.<sup>[3]</sup>

It is also interesting to discover whether the catalytically active species is formed in a reversible or irreversible manner with TBHP. Complex **7** was therefore treated with a 200-fold excess of TBHP (5.5M in *n*-decane solution, the same conditions as applied in our catalytic examinations) in  $\text{CH}_2\text{Cl}_2$ . After workup of the reaction mixture, we found that we obtained the starting complex unchanged (see also above). This provides additional support for the conclusions drawn in the previous section that the Mo–X bonds are not cleaved and indicates that the catalytically active species exists in equilibrium with the starting complex in solution.

In order to try to get some information on the nature of this catalytic active species, the reaction of compound **7** with TBHP was then examined with spectroscopic tools. As the catalytic reactions are usually carried out at  $55^\circ\text{C}$ , we examined the reaction at both room temperature and at  $55^\circ\text{C}$ . In the event, it was found that little difference was observed between the two temperatures and therefore the results presented are from room temperature NMR, IR, and Raman studies.

$^{95}\text{Mo}$  NMR spectroscopy was explored as a tool to elucidate the electronic differences of the Mo core on reaction with TBHP. This involved sequential addition of TBHP solution in *n*-decane to a  $\text{CDCl}_3$  solution of the complex. Up to a threefold excess of TBHP was added. Still, only a slight change was observed in the  $^{95}\text{Mo}$  NMR spectra. The molybdenum signal occurred at  $\delta$  ( $^{95}\text{Mo}$ ) = 206, and is shifted only 16 ppm downfield relative to the signal of compound **7**. However, it is known that  $^{95}\text{Mo}$  NMR is not very sensitive to subtle changes in the coordination sphere. Therefore, the

reaction with TBHP might lead to a complex with a comparable  $^{95}\text{Mo}$  shift, as found for complex **7**.

It turned out that  $^1\text{H}$  NMR spectroscopy was a more informative analytical tool when the bipyridine aromatic  $^1\text{H}$  NMR signals were used as diagnostic features. The addition of 0.5 equivalents of TBHP leads to new signals of very low intensity (See Table 5). Increasing the amount of TBHP leads to a concomitant increase in intensity of these new signals. When a 10:1 ratio of TBHP to complex **7** is used, the ratio of the  $^1\text{H}$  NMR signal intensity of compound **7** to the newly formed compound is  $\approx 3:1$ . We were initially concerned that these new signals were caused by ligand oxidation. However, this was proven not to be the case (see Table 5).

Table 5. Aromatic  $^1\text{H}$  NMR signals of 4,4'-bis(*n*-hexyl)bipyridine in selected compounds (in  $\text{CDCl}_3$ ).

Compound <b>7</b>	9.39	8.06	7.49
<b>7</b> + TBHP	8.82	8.01	7.30
<i>N</i> -oxide	8.22	7.50	7.14
$[\text{MoO}_2\text{X}_2(\text{N-oxide})]$	8.54	7.56	7.52
protonated ligand	8.75	8.34	7.38
free ligand	8.52	8.21	7.09

Moreover, it was found that 4,4'-bis(*n*-hexyl)-2,2'-bipyridine-*N*-oxide ligands coordinate to  $[\text{MoO}_2\text{Cl}_2]$  in a 1:2 stoichiometry. We were also concerned that the TBHP proton was transferred to the Lewis base ligand. Thus, the free ligand was protonated with TFA, but the aromatic  $^1\text{H}$  NMR signals of the protonated species were found at different NMR shifts (Table 5). Therefore, protonation of the Lewis base ligand may be excluded. It can also be assumed that protonation of the Lewis base ligand would destabilize the complex resulting in its decomposition, a phenomenon which was not observed. The overall upfield shift of the aromatic  $^1\text{H}$  signals from the free complex to the anomalous signals observed on treatment with TBHP could indicate a somewhat less Lewis acidic molybdenum core. This may be expected in case of coordination of the TBHP to the molybdenum.

$^{17}\text{O}$  NMR experiments were also found to be quite informative on the reaction between  $[\text{MoO}_2\text{Cl}_2(\text{alkylbipy})]$  and TBHP.  $^{17}\text{O}$ -Labeled complex **7** exhibits a signal at  $\delta = 995$  with a linewidth of 800 Hz. On the addition of 0.5 equivalents of TBHP, a new low-intensity signal appears at  $\delta = 563$  that has a linewidth of 100 Hz (measurement time was  $\approx 15$  min). The signal increases in intensity on the addition of more TBHP. The M=O signal does not change significantly on the incremental addition of TBHP and the linewidth remains constant. Unlabeled TBHP itself reveals two broad signals at  $\delta = 251$  and 202 with linewidths of 800 and 1050 Hz, respectively, which were not observed in the  $^{17}\text{O}$  NMR spectra. Molybdenum peroxo complexes exhibit their peroxo signals in a range of  $\delta = 400$ – $600$  with linewidths of 1200–2000 Hz.<sup>[19b]</sup> In our experiments, neither the chemical shift nor the linewidth were found to change for the signal at  $\delta = 563$ . Considering the fact that the TBHP oxygen atoms are not evident in the NMR spectra, it is highly unlikely that the peak at  $\delta = 563$  is caused by a minor amount of TBHP coordinated to the Mo center. Therefore, we believe that this oxygen signal

can be attributed to a labeled oxygen of the complex. We propose that the proton of the TBHP is transferred to an oxygen of the complex upon coordination of the TBHP to the molybdenum core. From a literature precedent, the linewidth of  $\approx 100$  Hz is evidently too narrow for a molybdenum peroxy species and a Mo- $^{17}\text{O}-\text{H}$  is a reasonable assignment. However, to the best of our knowledge  $^{17}\text{O}$  NMR spectra of Mo $^{\text{VI}}$ -OH moieties have not yet been reported in the literature.

Solution-phase IR and Raman spectroscopy was used to examine the changes in the stretching frequencies on reaction of the complex with TBHP solutions in THF and  $\text{CH}_2\text{Cl}_2$ . The terminal Mo=O bonds of complex **7** show characteristic *cis* Mo=O stretching frequencies at  $\tilde{\nu} = 942$  and  $915\text{ cm}^{-1}$ . Small spectral changes are observed after addition of 0.5 equivalents of TBHP, which become clear and pronounced after the addition of a tenfold excess of TBHP to the complex. A new band at  $\tilde{\nu} = 978\text{ cm}^{-1}$  increases in intensity on addition of TBHP to a solution of complex **7**. Additionally, two other bands at  $\tilde{\nu} = 885$  and  $593\text{ cm}^{-1}$  appear in both the IR and Raman spectra. The peaks attributable to the Mo=O stretching frequencies are found to decrease in intensity. The new bands can be reasonably assigned to the  $\eta^1$ -coordinated *t*BuOO $^-$  species and a protonated Mo=O. The new band at  $980\text{ cm}^{-1}$  correlates to  $\nu(\text{M}=\text{O})$ , the band at  $885\text{ cm}^{-1}$  to  $\nu(\text{O}-\text{O})$ , and the signal at  $593\text{ cm}^{-1}$  to the  $\nu(\text{Mo}-\text{O})$ . Mimoun et al. reports similar bands for the vanadium(v)  $\eta^1$ -peroxy complex,  $[\text{VO}(\text{dipic})(\text{OO}t\text{Bu})]$  (dipic = 2,6-pyridinedicarboxylate).<sup>[19c]</sup> The latter complex exhibits a band at  $980\text{ cm}^{-1}$  attributed to the terminal V=O, whereas the  $\nu(\text{O}-\text{O})$  stretching band occurs at  $890\text{ cm}^{-1}$  and the  $\nu(\text{V}-\text{O})$  at  $580\text{ cm}^{-1}$ . Molybdenum mono- and bisperoxy species have also been reported in the literature.<sup>[2n, 19d]</sup> The complex  $[\text{MoO}(\text{O}_2)\text{Cl}_2\text{L}_2]$  (L = DMF, HPMT) shows the  $\nu(\text{O}-\text{O})$  band at  $920\text{ cm}^{-1}$ , whilst two bands at  $550$  and  $600\text{ cm}^{-1}$  are found for the Mo(O $_2$ ) stretching frequencies.  $[\text{MoO}(\text{O}_2)_2\text{L}_2]$  (L = range of mono and bidentate N/O ligands) exhibit their peroxy  $\nu(\text{O}-\text{O})$  at  $880\text{ cm}^{-1}$  and the  $\nu(\text{Mo}-\text{O})$  is highlighted by two bands at  $500$  and  $600\text{ cm}^{-1}$ . Since analogous bands are not found in our experiments, we can confidently exclude the possibility of the formation of a  $\eta^2$  mono- or bisperoxy species. A shoulder that appears in the IR spectra at approximately  $3270\text{ cm}^{-1}$  on addition of one equivalent of TBHP broadens ( $3300\text{ cm}^{-1}$ ) after the addition of excess TBHP to the complex solution. This is suggestive of a different OH species to that of TBHP-OH. We were concerned that this might merely be caused by moisture in the sample. However, the presence of moisture would be confirmed by a band at  $\nu \approx 1600\text{ cm}^{-1}$ . This band was conspicuously absent. Thus, it is reasonable to assume that the  $3300\text{ cm}^{-1}$  band can be ascribed to a Mo-OH vibration.

We were also interested in gaining information on the mode of coordination of the TBHP to the molybdenum center, namely whether initial protonation of a Mo=O occurs followed by coordination of the *t*BuOO $^-$  or coordination of the TBHP to the Mo is the first step followed by proton transfer to the M=O. We examined the reaction between complex **7** and TFA and it was found that no changes occurred in the  $^1\text{H}$  NMR spectrum, even after two days. Complex decomposition was not observed. This suggests that the

Mo=O is not sufficiently basic to be protonated even by such a strong acid. It is also argued that the triflate anion has an insufficient coordinating ability on account of the electron-withdrawing capacity of the  $\text{CF}_3$  group. This strongly suggests that coordination of the TBHP is a prerequisite for proton transfer. Considering the  $\text{p}K_{\text{a}}$  of TBHP ( $\approx 11$ ), it was decided to compare its coordination with an alcohol of similar  $\text{p}K_{\text{a}}$ . Phenol was chosen, having a  $\text{p}K_{\text{a}}$  of 10. It was found that the phenol  $^1\text{H}$  NMR signals remained unchanged on reaction with complex **7** and the phenolic O-H was still evident. It might be that the phenol is too sterically demanding to coordinate to the molybdenum core and, as proton transfer is not observed, then it may be assumed that coordination of the alcohol is required before the Mo=O may be protonated. Experiments with radical scavengers showed that radical species which are not extremely short lived seem not to be involved in the catalytic process.

**Theoretical studies:** DFT calculations<sup>[20]</sup> (ADF program<sup>[21]</sup>) were performed in order to have a clearer idea of the first steps in the mechanism of olefin oxidation in the presence of Mo $^{\text{VI}}$  catalysts and TBHP and, in particular, to see whether or not a theoretical study supports the spectroscopic examinations concerning the mechanism. Although there are previous theoretical studies, most of them are either relatively old and used semiempirical methods, which are not particularly suited to address all the aspects of the problem,<sup>[22]</sup> or dealt with catalytic systems that are significantly different from the present one, preventing the extrapolation of conclusions.<sup>[23, 18g]</sup>

The precursor complexes described above are octahedral derivatives of *cis*-dioxomolybdenum(vi), which have already been theoretically addressed,<sup>[24, 2e, j]</sup> the *cis* preference being assigned to the increased  $\pi$  donation into the empty  $t_{2g}$  orbitals of the  $d^0$  metal center.<sup>[24a]</sup> In the family of complexes  $[\text{MoO}_2\text{X}_2\text{L}_2]$ , the *cis,trans,cis* arrangement was found to be more stable than the all-*cis* one, especially when bulky ligands are present, and is found for most structures.<sup>[24d]</sup> Thus, it is this geometry that is exhibited by the catalytic precursors  $[\text{MoO}_2\text{X}_2\text{L}_2]$ , in which X = halogen, Me, and L $_2$  = a bidentate nitrogen ligand (see X-ray description).  $[\text{MoO}_2\text{Br}_2(2,2'\text{-bipyridine})]$  (**2**) was chosen for initial calculations and its geometry was fully optimized by means of the ADF program and two basis sets of different quality [I (smaller) and II (larger)]; see the Experimental Section]. Symmetry was constrained to be  $C_{2v}$ . Similar calculations were also performed for the dichloro and the dimethyl derivatives, **1** and **3**.

The optimized geometries of complex **2** are shown in Figure 2, for basis set I (left) and II (right), with bond distances ( $\text{\AA}$ ) and angles ( $^\circ$ , italics). As is typical, the complex

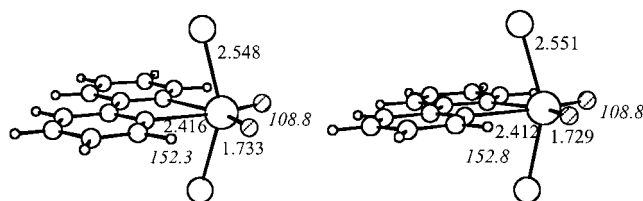


Figure 2. The optimized geometries (bond lengths [ $\text{\AA}$ ] and angles [ $^\circ$ , italics]) of  $[\text{MoO}_2\text{Br}_2(2,2'\text{-bipy})]$  (**2**) with basis set I (left) and II (right).

adopts a distorted octahedral geometry. The angle between axial ligands is very far from the ideal  $180^\circ$ .

The two geometries obtained are very similar, in spite of the different basis sets used. It is also important to check how they compare with available experimental structures of this type of compounds, which were described in detail above (Table 3).

The calculated values for **2** show good agreement with the experimental values, namely Mo–O bond lengths (calculated 1.733, 1.729 Å, for both basis sets; experimental 1.711, 1.728 Å), Mo–N bond lengths (calculated 2.416, 2.412 Å; experimental 2.317, 2.293 Å), and Mo–Br bond lengths (calculated 2.548, 2.551 Å; experimental 2.511, 2.524 Å). Concerning the Br–Mo–Br and O–Mo–O angles, the following values were found:  $152.3^\circ$  (basis set I),  $152.8^\circ$  (basis set II),  $158.96^\circ$  (exptl), and  $108.8^\circ$  (basis set I),  $108.8^\circ$  (basis set II),  $106.9^\circ$  (exptl), respectively. The angle involving the *cis*-oxygen atoms is widened in the calculations, while the opposite happens for the Br–Mo–Br angle. The chelate N–Mo–N angle becomes smaller by  $\approx 3^\circ$  in the calculations. The effect of the basis set on the quality of the structure is not significant, as the tendency in both cases is for slightly longer bond lengths.

These data suggest that there is no significant improvement in the quality of the calculations by using the larger basis set, and therefore the smaller basis set, which still contains a polarization function for nonmetals and saves computational time, was chosen for the remaining ADF calculations.

Frequency calculations were performed in order to compare the assignment of the experimental IR and Raman spectra. The B3LYP method in Gaussian98 was used for convenience.<sup>[25]</sup> The frequency calculations were preceded by a full structure optimization of the three complexes under study (**1**, **2**, **3**) with two different basis sets of different quality, 3-21G and 3-21G\*, for all atoms. The final structures are very similar to those described above and the experimental ones, the effect of the larger basis set being reflected in the Mo–Br distance (2.571 Å with 3-21G, 2.505 Å with 3-21G\*, and 2.511, 2.524 Å in the experimental). As the frequencies obtained from the two calculations were not very different, only the results relative to the larger basis set will be reported below.

The calculated frequencies (B3LYP, see below) for the bipy complexes are given in Table 6. Although the numbers do not agree completely, the trends fit the experimental values, the Mo–N stretching frequencies being the weakest and more difficult to assign. The Mo=O frequencies are closer than those observed experimentally, and appear at higher wavenumbers, while the agreement between experimental and

calculated values for the asymmetric Mo–X stretching vibration and the Mo–C frequencies is much better. The quality of the basis set, the theoretical method used, and the fact that a gaseous molecule is analyzed for the calculations may be responsible for the partial agreement.

Several different reactions between  $[\text{MoO}_2\text{X}_2\text{L}_2]$  complexes and TBHP may be postulated, as described above. According to the spectroscopic examinations, it is assumed that the first step of the catalytic cycle ends with the formation of an intermediate (possibly the catalytically active species) containing coordinated  $\text{RCOO}^-$  and a protonated ligand. Possible limiting mechanisms consist of either protonation of one ligand (one oxide or one N atom of the bidentate ligand), followed by coordination of the  $\text{ROO}^-$  anion, or of a more concerted process, where approach of  $\text{RCOOH}$  leads to protonation of a ligand and coordination of the  $\text{RCOO}^-$  anion.

In order to choose among these possibilities and to see whether they are reasonable to be considered as the initiating steps, protonation at the O and N atoms were first studied with DFT calculations (ADF), starting from complex **2**. The structure obtained after full geometry optimization when complex **2** is protonated at one of the oxygen atoms (they are equivalent), to form  $[\text{MoO}(\text{OH})\text{Br}_2(\text{bipy})]^+$ , is shown in Figure 3, with indication of the most relevant bond lengths and angles.

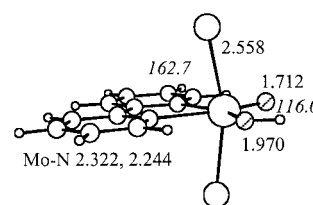


Figure 3. The optimized structure (bond lengths [Å] and angles [ $^\circ$ , italics]) of  $[\text{MoO}(\text{OH})\text{Br}_2(2,2'\text{-bipy})]^+$  obtained from **2**, after protonation at one of the oxygen atoms.

A comparison with the parent compound reveals in the new species  $[\text{MoO}(\text{OH})\text{Br}_2(2,2'\text{-bipy})]^+$  (see Figure 3), the weakening of the Mo–O bond involving the protonated oxygen atom, a widening of the Br–Mo–Br angle, which leads to asymmetry of the two Mo–N bonds and is caused by the different *trans* influences of O and OH, and shorter Mo–N bonds. A similar calculation for the species protonated at one of the nitrogen atoms of the bipy ligand led to the formation of a tetrahedral derivative of  $\text{Mo}^{\text{VI}}$ , the protonated bipy moving away from the coordination sphere of molybdenum. This alternative was therefore discarded.

The next option was to allow the approach of the  $\text{MeOO}^-$  anion (used as a model for  $t\text{BuOO}^-$ ) to the metal to form the heptacoordinated species  $[\text{MoO}(\text{OH})\text{Br}_2(2,2'\text{-bipy})(\text{MeOO})]$ . Considering the distorted octahedral geometry of the starting complex, the sterically less constrained directions of approach for an incoming ligand are from above the center of a face. There are four types of faces in the octahedron, since the O–Mo–O plane is a symmetry

Table 6. Calculated (B3LYP) frequencies for the three  $[\text{MoO}_2\text{X}_2(\text{bipy})]$  complexes.

	<b>1</b> (Cl)		<b>2</b> (Br)		<b>3</b> (Me)	
	IR, Raman	Raman	IR, Raman	Raman	IR, Raman	Raman
MoO <sub>2</sub> sym. str.	986 s		966 s		975 s	
MoO <sub>2</sub> asym. str.	976 s		976 s		966 s	
MoC <sub>2</sub> asym. str.	–	–	–	–	503 m	
MoC <sub>2</sub> sym. str.	–	–	–	–	468 m	
MoX <sub>2</sub> asym. str.	336 s		287 s		–	–
MoX <sub>2</sub> sym. str.	293 w			208 w	–	–
MoN <sub>2</sub> sym. str.	246 w		nc <sup>[a]</sup>		240 w	
MoN <sub>2</sub> asym. str.	186 w		186 vw		nc <sup>[a]</sup>	

[a] nc = not calculated.



plane, defined as (OH)OBr (**A**), (OH)NBr (**B**), ONBr (**C**), and NNBr (**D**). The relative energies of the complexes formed after allowing  $\text{MeOO}^-$  to approach and optimizing the structure are 2.1, 0.0, 8.1, and 4.3  $\text{kcal mol}^{-1}$ , respectively. The final structures are shown in Figure 4. It is interesting to note how the already distorted octahedral coordination is further disturbed by the binding of the seventh ligand. In the lowest energy structures (**A** and **B**), there is a hydrogen bond assistance, which helps to stabilize those forms. The H(O) approaches one oxygen of the  $\text{MeOO}$  group in a  $\text{O-H}\cdots\text{O}$  arrangement. In **A**, the hydrogen bond is formed between the O-H group and the oxygen of the peroxide attached to Mo ( $\text{O}\cdots\text{H}$  distance 2.032 Å). In **B**, the hydrogen bond involves the  $\beta$  oxygen of OOMe ( $\text{O}\cdots\text{H}$  distance 1.572 Å), an aspect to which we shall return later.

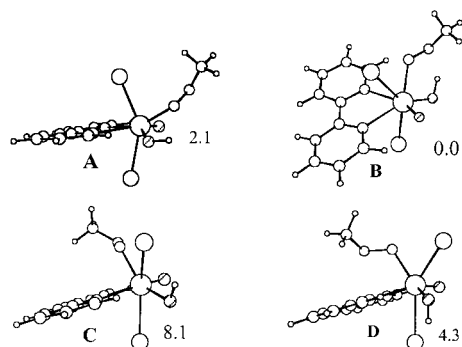


Figure 4. Optimized geometries and relative energies [ $\text{kcal mol}^{-1}$ ] of the heptacoordinated species  $[\text{MoO}(\text{OH})\text{Br}_2(2,2'\text{-bipy})(\text{MeOO})]$  formed when the  $\text{MeOO}^-$  anion approaches  $[\text{MoO}(\text{OH})\text{Br}_2(2,2'\text{-bipy})]^+$  from above face (OH)OBr (**A**), (OH)NBr (**B**), ONBr (**C**), and NNBr (**D**).

To confirm the reliability of these results, we attempted to reach the same intermediates through another route, namely by optimizing the geometry of complex **2** in the presence of the HOOMe molecule. It was necessary to constrain the Mo-O (from HOOMe) and O-O distances to remain constant, otherwise the two species would not stay together. The approach of  $\text{MeOOH}$  took place as shown schematically in Figure 5 for the ONBr face (**F**).

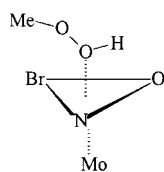


Figure 5. Schematic diagram showing the approach of HOOMe to the ONBr face of  $[\text{MoO}_2\text{Br}_2(2,2'\text{-bipy})]$ .

This partial optimization was followed by a full optimization and this procedure was applied to the three nonequivalent faces of **2**. In the absence of an OH group, there are only three independent faces OOBr (**E**), ONBr (**F**), and NNBr (**G**). The approaches along **E** and **G** (not shown) led to fragmentation of the molecule; only **F** led to a converged structure (Figure 6 left). It was found that during the optimization, the hydrogen atom of the peroxide was trans-

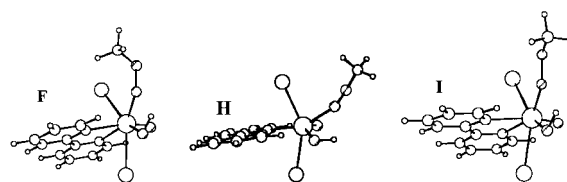


Figure 6. Optimized geometries of the heptacoordinated species  $[\text{MoO}(\text{OH})\text{Br}_2(2,2'\text{-bipy})(\text{MeOO})]$  formed when HOOMe approaches  $[\text{MoO}_2\text{Br}_2(2,2'\text{-bipy})]$  from above face ONBr (**F**), starting at different Mo-O distances.

ferred to one oxide. The final geometry is very similar to **B** (Figure 4). The same approach was repeated starting from different fixed initial Mo-O distances (1.9 Å, **H**, and 2.1 Å, **I**, instead of 2.0 Å as before). The new geometries are given in Figure 6, center and right. These final geometries are very similar to those obtained with the first methodology, both in energy and geometry (Figure 6). They differ essentially by the orientation of the OOMe group. An  $\text{O-H}\cdots\text{O}$  hydrogen bond is present in all the structures.

The lowest energy species corresponds to the form **B**. The most relevant features are given in Figure 7, in two views emphasizing different aspects. From these results, it can be inferred that the most likely intermediate should exhibit a coordination number of seven for molybdenum in a face-capped octahedral structure, with a hydrogen bond, which for this intermediate involves the  $\beta$ -hydrogen of the peroxide. This geometry is somewhat different from that of a characterized vanadium complex,  $[\text{VO}(\text{dipic})(\text{OO}t\text{Bu})(\text{H}_2\text{O})]$ .<sup>[23a]</sup> In the Mo complex, the coordination number is already seven for  $\eta^1$ -peroxide, therefore the second  $\text{Mo}\cdots\text{O}$  distance is outside the bonding range.

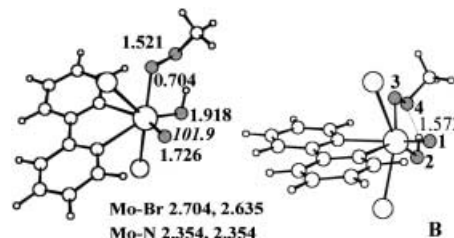


Figure 7. Two different views of the optimized geometry of the lowest energy heptacoordinated species  $[\text{MoO}(\text{OH})\text{Br}_2(2,2'\text{-bipy})(\text{MeOO})]$ .

These calculations were repeated under similar conditions for the Cl and Me complexes and comparable results were obtained, the same intermediate being favored. After detecting the intermediate for this first reaction step, an attempt was made to identify the transition state. This was achieved with Gaussian98 (B3LYP method, as described above for the frequency calculations), and a model of the complex in which the bipy ligand was replaced by diazabutadiene. Locating transition states presents difficulties and it is important that the method used is reliable. Preliminary calculations were thus performed on the complex  $[\text{MoO}_2\text{Cl}_2(\text{N}_2\text{C}_2\text{H}_2)]$ , since a crystal structure<sup>[7a]</sup> and previous theoretical studies are available.<sup>[2c-i]</sup>

The same basis set used by Barea et al.<sup>[2c]</sup> led to a reasonable agreement with the experimental structure. It was also tested on the Br derivative since this was the system

under study, as described above, and compared with the results obtained with the basis set (3-21G\*) used. When this latter set was used, contraction of bonds was observed making them even closer to experimental values.

The geometries of the reagents ( $[\text{MoO}_2\text{Br}_2(\text{N}_2\text{C}_2\text{H}_2)]$  and  $\text{MeOOH}$ ), the transition state, and the final product (the reaction intermediate, which we assume to be the catalytic active species, as was described before), as well as their energies, are shown in Figure 8. Another stationary point,

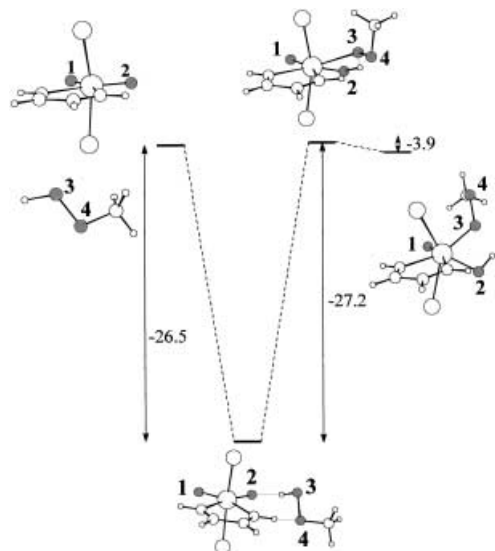


Figure 8. Stationary points, transition state, and relative energies [ $\text{kcal mol}^{-1}$ ] along the reaction path between  $[\text{MoO}_2\text{Br}_2(\text{N}_2\text{C}_2\text{H}_2)]$  (2) and  $\text{HOOMe}$  to form  $[\text{MoO}(\text{OH})\text{Br}_2(\text{N}_2\text{C}_2\text{H}_2)(\text{MeOO})]$ .

which can be described as a weakly bound complex between the two reagents, was also found across the reaction pathway and occupies an energy minimum. The structural changes experienced by the molybdenum coordination sphere when this adduct is formed are minimal and its stability can be ascribed to the formation of two hydrogen bonds,  $\text{O}_3\text{--H}\cdots\text{O}_2$  and  $\text{N--H}\cdots\text{O}_4$  between the two reagents, with  $\text{H}\cdots\text{O}_{2,4}$  distances of 1.67 and 1.68 Å, respectively. While the first one should also be found in the real system, the  $\text{N--H}\cdots\text{O}_4$  interaction is a feature of the model, as bipy has been replaced by  $\text{N}_2\text{C}_2\text{H}_2$ , so that in the active system such an adduct should not be so stable.

The transition state was determined as described in the Experimental Section and the existence of one imaginary frequency was detected. The  $\text{O}_3\text{--H}\cdots\text{O}_2$  interaction has developed in such a way that the hydrogen has almost been transferred from the peroxide ( $\text{O}_3$ ) to the molybdenum complex ( $\text{O}_2$ ). The  $\text{O}_3\cdots\text{H}$  distance has become 1.29 Å and  $\text{O}_2\cdots\text{H}$  1.17 Å, while  $\text{O}_3$  is already weakly bound to the metal. The  $\text{Mo--O}_3$  distance is 2.38 Å, but is depicted as a solid line in the picture. The  $\text{N--H}\cdots\text{O}_3$  interaction remains ( $\text{O}_3\cdots\text{H}$  1.69 Å). The  $\text{O}_1\text{--Mo--O}_2$  angle narrows, from  $\approx 107^\circ$  in the reagent and the adduct, to  $97.1^\circ$  in the final state. In the evolution to the product, the  $\text{Mo--O}_3$  and  $\text{O}_2\text{--H}$  distances decrease to 2.05 and 1.01 Å, respectively, typical bond lengths, and the molybdenum becomes heptacoordinate. The  $\text{N--H}\cdots\text{O}_3$  hydrogen bond vanishes. Although this product is slightly different from the intermediate in the

reaction described above (B in Figure 7), namely in the orientation of the methyl group and the consequent absence of the hydrogen bond between  $\text{O}_2\text{--H}$  and the  $\beta$  hydrogen  $\text{O}_4$ , the metal coordination sphere is essentially the same. This indicates that the calculation with the model leads to a similar result as that which used the bipy ligand. The activation energy is calculated to be  $+27.2 \text{ kcal mol}^{-1}$ . As discussed above, there is a  $\text{N--H}\cdots\text{O}$  hydrogen bond both in the adduct and in the transition state that should not be found in the real system since bipy and the other nitrogen ligands used in the experiments do not contain a  $\text{N--H}$  bond. The formation of an adduct stabilized only by the  $\text{O--H}\cdots\text{O}$  bond is, however, expected independently of the  $\text{N--N}$  ligand. Of course, one cannot be sure that the  $\text{N--H}\cdots\text{O}$  interaction will be the same in the adduct and in the transition state, so that this will affect the estimation of the activation energy.

IRC (internal reaction coordinate) calculations were performed to check whether the transition state led both to reagents and products.

## Conclusions

Complexes of the general formula  $[\text{MoO}_2\text{X}_2\text{L}_2]$  ( $\text{L}_2 = \text{bipy}$ ,  $\text{bpym}$ , diazabutadienes, etc.) are moderately active epoxidation catalysts. They have very distinctive chemical shifts both in  $^{95}\text{Mo}$  and  $^{17}\text{O}$  NMR spectra. Their structures can be described both as distorted octahedra or as regular octahedra with a displaced central metal. Their catalytic activity depends both on the ligands  $\text{L}$  and  $\text{X}$ . The highest activities are usually reached with  $\text{X} = \text{Cl}$  ligands, the lowest with  $\text{X} = \text{Me}$  ligands if the ligand  $\text{L}$  remains unchanged. The oxidizing agent TBHP is transformed to *tert*-butyl alcohol during the course of the reaction. This byproduct slows down the reaction velocity since it can also coordinate to the molybdenum center. The first step of the catalytic cycle is the reaction of TBHP with  $[\text{MoO}_2\text{X}_2\text{L}_2]$ . The HOO proton is transferred to one of the terminal oxygen atoms and the  $^-\text{OOR}$  group coordinates as seventh ligand in a  $\eta^1$  manner to the Mo center. This addition takes place on the NOX face of the octahedron and promotes the activation of the TBHP. Alternative protonation of the bidentate nitrogen donor ligand or of the  $\text{X}$  ligand under HX elimination do not take place under the applied reaction conditions. The second step of the reaction should proceed, as proposed by other authors<sup>[23b,fj]</sup> by approach of the olefin to the coordinated  $\alpha$  oxygen. At this stage, it is important to recall that the intermediate calculated with the bipy ligand (Figure 7) exhibits a hydrogen bond between the  $\beta$ -oxygen and the coordinated OH group; this will favor the formation of an epoxide and release of the alcohol to leave the precursor complex  $[\text{MoO}_2\text{X}_2\text{L}_2]$ . These features are summarized in Figure 9. The catalyst precursor can be recovered unchanged after the catalytic cycle.

It is interesting to note that a preference for a quite similar mechanism was already proposed about 20 years ago for complexes containing the  $\text{Mo=O}$  moiety, but no convincing experimental evidence was available.<sup>[2p]</sup> At least for complexes of the type  $[\text{MoO}_2\text{X}_2\text{L}_2]$  this proposal is now shown to be in agreement with the experimental findings.

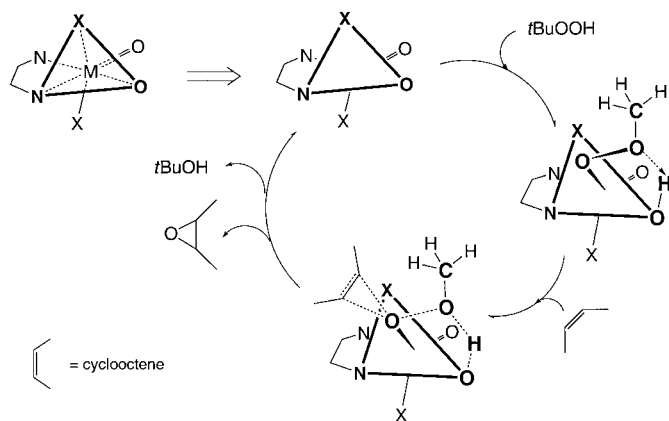


Figure 9. Proposed reaction mechanism for *t*BuOOH activation and olefin epoxidation taking place at the NOX face of octahedral  $[\text{MoO}_2\text{X}_2\text{L}_2]$  ( $\text{X} = \text{Cl}, \text{Br}, \text{Me}$ ) complexes. In the drawings the metal is hidden behind the face for clarity.

## Experimental Section

All preparations and manipulations were performed with standard Schlenk techniques under an atmosphere of nitrogen. Solvents were dried by standard procedures (THF, *n*-hexane and  $\text{Et}_2\text{O}$  over Na/benzophenone;  $\text{CH}_2\text{Cl}_2$  and NCMe over  $\text{CaH}_2$ ), distilled under argon and kept over 4 Å molecular sieves (3 Å for NCMe). Microanalyses were performed at the ITQB and the Mikroanalytische Labor of the Technical University of Munich (M. Barth). Powder XRD data were collected on a Phillips X'pert diffractometer with  $\text{CuK}\alpha$  radiation filtered by Ni.  $^1\text{H}$  NMR spectra were recorded at 300 MHz and 400 MHz on Bruker CXP 300 and Bruker Avance DPX-400 spectrometers, respectively.  $^{13}\text{C}$  NMR spectra were measured at 100.28 MHz on a JEOL JNM GX-400 and a Bruker Avance DPX-400,  $^{17}\text{O}$  NMR spectra were measured at 54.14 MHz on a BRUKER GX-400, and  $^{95}\text{Mo}$  NMR spectra were measured at 26.07 MHz on a Bruker Avance DPX-400.  $^{17}\text{O}$  enrichment of the oxo group in complexes  $[\text{MoO}_2\text{X}_2(\text{DMF})_2]$  ( $\text{X} = \text{Br}, \text{Cl}$ ) was carried out by treatment of a solution of the unlabeled complex in  $\text{CH}_2\text{Cl}_2$  with excess  $\text{H}_2^{17}\text{O}$ , in a manner analogous to that previously reported.<sup>[20]</sup> The labeled complexes  $[\text{Mo}^{17}\text{O}_2\text{X}_2(\text{NCMe})_2]$  ( $\text{X} = \text{Br}, \text{Cl}$ ) were then obtained by recrystallization of  $[\text{Mo}^{17}\text{O}_2\text{Cl}_2(\text{DMF})_2]$  from NCMe. IR spectra of solid samples (in the form of KBr pellets and Nujol mulls) were measured on a Bio-Rad FTS-60A. The far IR spectra of the complexes were recorded as Nujol mulls on a Bio-Rad FTS-175A system equipped with a 6 mm Mylar beamsplitter. The Raman spectra were also performed with a Bio-Rad dedicated FT-Raman spectrometer with the 1064 nm excitation of a Nd-YAG laser. Force-constant calculations have been performed by a program system developed by J. Mink based on a simplified model of introducing internal coordinates.

$[\text{MoO}_2\text{X}_2]$  ( $\text{X} = \text{Br}$  or  $\text{Cl}$ )<sup>[26]</sup>  $[\text{MoO}_2\text{X}_2(\text{NCMe})_2]$  ( $\text{X} = \text{Br}$  or  $\text{Cl}$ )<sup>[3a]</sup>  $[\text{MoO}_2\text{Br}_2(\text{bipyrimidine})]$ ,<sup>[3a]</sup>  $[\text{MoO}_2\text{Me}_2(\text{bipyrimidine})]$ ,<sup>[3a]</sup>  $[\text{MoO}_2\text{Me}_2(\text{bipyridine})]$ ,<sup>[4a]</sup>  $[\text{MoO}_2\text{Br}_2(\text{bipyridine})]$ ,<sup>[9, 27]</sup>  $[\text{MoO}_2\text{Cl}_2(\text{bipyridine})]$ ,<sup>[28]</sup> were prepared according to published processes with only minor changes. The elementary analysis was correct in all cases, the spectroscopic data were in accord with those given in the literature.

**Preparation of 4,4'-dihexyl-2,2'-bipyridine:** *n*BuLi in *n*-hexane (17.5 mL, 28 mmol, 1.6 M) was added dropwise to a solution of diisopropyl amine (3.9 mL, 28 mmol) in THF (10 mL) at 0 °C. 4,4'-Dimethyl-2,2'-bipyridine (2 g, 11 mmol) dissolved in THF (50 mL) was added slowly to the reaction mixture and the resulting red solution was stirred at 0 °C for 3 h. A solution of amyl bromide (3.5 mL, 28 mmol) was then added, and the reaction was stirred overnight and allowed to slowly reach room temperature. The reaction was quenched by the addition of methanol and the solution was poured onto ice. The crude product was extracted with  $\text{Et}_2\text{O}$  and purified by chromatography (silica,  $\text{EtOAc}/\text{hexane}$  40:60) to yield the pure product as a pale yellow oil. Yield: 2.5 g (70 %);  $^1\text{H}$  NMR (400 MHz,  $\text{CDCl}_3$ ):  $\delta = 0.84$  (m, 6H;  $\text{CH}_3$ ), 1.19 (m, 4H;  $\text{CH}_2$ ), 1.27 (m, 8H;  $(\text{CH}_2)_2$ ), 1.65 (m, 4H;  $\text{CH}_2$ ), 2.64 (m, 4H;  $\text{CH}_2$ ), 7.09 (m, 2H; py-H), 8.21 (m, 2H; py-H), 8.52 (m,

2H; py-H); elemental analysis calcd (%) for  $\text{C}_{22}\text{H}_{32}\text{N}_2$  (324.51): C 81.43, H 9.94, N 8.63; found: C 81.12, H 9.84, N 9.04

**Preparation of  $[\text{MoCl}_2\text{O}_2(\text{bipyrimidine})]$  (4):** A solution of  $[\text{MoO}_2\text{Cl}_2(\text{NCMe})_2]$  (0.10 g, 0.38 mmol) in NCMe (15 mL) was treated with bipyrimidine (0.06 g, 0.38 mmol), and the mixture was vigorously stirred for 40 min. The resulting yellow solution was evaporated to dryness, and a pale yellow microcrystalline powder was formed. Yield: 96 %; IR (KBr):  $\tilde{\nu} = 3086$  (m), 3007 (m), 1574 (s), 1550 (s), 1409 (vs), 1211 (m), 1103 (m), 1013 (m), 943 (vs), 909 (vs), 824 (s), 758 (s), 688 (m),  $655\text{ cm}^{-1}$  (s);  $^1\text{H}$  NMR ( $\text{CD}_3\text{CN}$ , 400 MHz, 20 °C):  $\delta = 9.65$  (d, 2H), 9.37 (d, 2H), 7.98 (m, 2H); elemental analysis calcd (%) for  $\text{C}_8\text{H}_6\text{Cl}_2\text{MoN}_4\text{O}_2$  (357.01): C 26.92, H 1.69, N 15.69; found: C 26.91, H 1.70, N 15.50.

**Preparation of  $[\text{MoO}_2\text{Cl}_2(n\text{-hexylbipy})]$  (7):** 4,4'-Dihexyl-2,2'-bipyridine (0.842 g, 2.60 mmol) was added to a suspension of  $[\text{MoO}_2\text{Cl}_2]$  (0.469 g, 2.36 mmol) in  $\text{CH}_2\text{Cl}_2$  (5 mL) and the resulting solution was stirred for 30 mins. The solution was filtered and concentrated to 1 mL. Hexane was added to precipitate the colorless product, which was purified by washing with hexane. The colorless solid was collected and dried *in vacuo* to yield the title complex. Yield: 1.19 g (96 %); IR (KBr):  $\tilde{\nu} = 3071$  (w), 2939 (s), 1610 (s), 937 (vs), 912 (vs), 895 (m), 623 (w), 344 (m),  $237\text{ cm}^{-1}$  (m);  $^1\text{H}$  NMR (400 MHz,  $\text{CDCl}_3$ ):  $\delta = 0.92$  (t, 6H;  $\text{CH}_3$ ), 1.36 (m, 8H;  $(\text{CH}_2)_2$ ), 1.43 (m, 4H;  $\text{CH}_2$ ), 1.76 (m, 4H;  $\text{CH}_2$ ), 2.84 (t, 4H;  $\text{CH}_2$ ), 7.50 (d, 2H; py-H), 8.06 (s, 2H; py-H), 9.39 (d, 2H; py-H); elemental analysis calcd (%) for  $\text{C}_{22}\text{H}_{32}\text{Cl}_2\text{MoN}_2\text{O}_2$  (523.36): C 50.49, H 6.16, N 5.35; found: C 50.80, H 6.40, N 5.16.

**$^{17}\text{O}$  labeling studies:** The labeled complexes  $[\text{Mo}^{17}\text{O}_2\text{Cl}_2(\text{DMF})_2]$  and  $[\text{Mo}^{17}\text{O}_2\text{Br}_2(\text{DMF})_2]$  were prepared according to the published procedure with  $\text{H}_2^{17}\text{O}$ .<sup>[29]</sup> IR (KBr):  $\tilde{\nu} = 941$  (s), 928 (vs), 904 (vs), 891 (s), 870 (vs),  $860\text{ cm}^{-1}$  (s) ( $\text{Mo}=\text{O}$ ). Labeled complexes  $[\text{Mo}^{17}\text{O}_2\text{Cl}_2(\text{NCMe})_2]$  and  $[\text{Mo}^{17}\text{O}_2\text{Br}_2(\text{NCMe})_2]$  were prepared by recrystallisation of  $[\text{Mo}^{17}\text{O}_2\text{X}_2(\text{DMF})_2]$  ( $\text{X} = \text{Cl}, \text{Br}$ ) from NCMe. Labeled complexes  $[\text{Mo}^{17}\text{O}_2\text{X}_2\text{L}]$  ( $\text{X} = \text{Cl}, \text{Br}, \text{Me}$  and  $\text{L} = \text{bipy}$  and  $\text{bpy}$ ) were prepared by the usual method with the labeled starting material  $[\text{Mo}^{17}\text{O}_2\text{X}_2(\text{NCMe})_2]$  ( $\text{X} = \text{Cl}, \text{Br}$ ).

**In-situ NMR experiments:** In a typical NMR experiment, portions of TBHP in *n*-decane ( $5.73 \times 10^{-5}$  M) were added with a microsyringe to a thermostated NMR vessel in a Schlenk tube under argon and containing a solution of the catalyst **7** (0.03 g,  $5.73 \times 10^{-5}$  mol) in  $\text{CDCl}_3$  (4.0 mL). After each addition, the NMR vessel was closed with a glass cap, transferred to a Bruker Avance DPX-400 spectrometer, and thermostated at the same temperature as the Schlenk tube was before. After a given time (5 min to 5 h to make sure that an equilibrium state has been reached),  $^1\text{H}$ ,  $^{95}\text{Mo}$ , and  $^{17}\text{O}$  NMR spectra were measured. After recording the spectra, a similar amount of TBHP was added by means of the same procedure and measured again.

### Crystallography

**Single-crystal structure determination:** Suitable single crystals for the X-ray diffraction studies were grown at room temperature by slow diffusion of diethyl ether into a solution of **1**, **2**, and **4** in dichloromethane. The reactant 2,2'-bipyridine (bipy) crystallized at ambient temperature from *n*-hexane/chloroform (1:3). The intensity data for **1**, **2**, and **4** were collected at 193 K and for bipy at 123 K. The selected crystals were coated with perfluorinated ether fixed in a capillary and transferred to the cold nitrogen stream (oxford Cryosystem). Preliminary examination and data collection for **1** and **4** were carried out on an imaging plate diffraction system (IPDS; Stoe&Cie) and for **2** and bipy on a kappa-CCD system (Nonius Mach3) equipped with a rotating anode (Nonius FR591) by graphite-monochromated  $\text{MoK}\alpha$  radiation.<sup>[30a,b]</sup> Data were corrected for Lorentz and polarization effects.<sup>[30b,c]</sup> All structures were solved by a combination of direct methods<sup>[30d]</sup> and difference Fourier syntheses. Full-matrix least-squares refinements were carried out by minimizing  $\sum w(F_o^2 - F_c^2)^2$  with SHELXL-97 weighting scheme and stopped at  $\text{shift}/\text{err} < 0.001$ .<sup>[30e]</sup> Neutral-atom scattering factors for all atoms and anomalous dispersion corrections for the non-hydrogen atoms were taken from the International Tables for X-Ray Crystallography.<sup>[30f]</sup> All calculations were performed on a DEC3000 AXP workstation and an Intel Pentium II PC with the STRUX-V system.<sup>[30g]</sup> Crystal data, intensity collection data, and refinement parameters are given in Table 3. A summary of the crystal structure determination is given in Table 7.

**Data collection and refinement for complex 1:** Data collection were performed within the  $\theta$  range of  $2.74^\circ < \theta < 25.88^\circ$  with an exposure time

Table 7. Selected crystallographic data for [MoO<sub>2</sub>Cl<sub>2</sub>(bipy)] (1), [MoO<sub>2</sub>Br<sub>2</sub>(bipy)] (2), [MoO<sub>2</sub>Cl<sub>2</sub>(bpym)] (4), and 2,2'-bipyridine (bipy).

	1	2	4	bipy
formula	C <sub>10</sub> H <sub>8</sub> Cl <sub>2</sub> MoN <sub>2</sub> O <sub>2</sub>	C <sub>10</sub> H <sub>8</sub> Br <sub>2</sub> MoN <sub>2</sub> O <sub>2</sub>	C <sub>8</sub> H <sub>6</sub> Cl <sub>2</sub> MoN <sub>4</sub> O <sub>2</sub>	C <sub>10</sub> H <sub>8</sub> N <sub>2</sub>
<i>M</i> <sub>r</sub> [g mol <sup>-1</sup> ]	355.03	443.93	357.01	156.18
habit/color	column/pale yellow	prism/pale yellow	prism/light brown	prism/colorless
crystal size [mm]	0.61 × 0.18 × 0.13	0.26 × 0.24 × 0.18	0.74 × 0.46 × 0.25	0.76 × 0.58 × 0.38
crystal system	triclinic	triclinic	monoclinic	monoclinic
space group	<i>P</i> $\bar{1}$ (No. 2)	<i>P</i> $\bar{1}$ (No. 2)	<i>C</i> 2/ <i>c</i> (No. 15)	<i>P</i> 2 <sub>1</sub> / <i>n</i> (No. 14)
<i>a</i> [Å]	8.331(1)	8.4045(5)	13.116(1)	5.4862(1)
<i>b</i> [Å]	8.536(1)	8.5185(4)	10.722(1)	6.1657(1)
<i>c</i> [Å]	9.788(2)	10.1839(6)	16.903(1)	11.6094(3)
$\alpha$ [°]	78.12(2)	77.650(3)		
$\beta$ [°]	82.41(2)	82.119(2)	108.94(1)	95.276(1)
$\gamma$ [°]	61.89(2)	62.584(3)		
<i>V</i> [Å <sup>3</sup> ]	600.3(2)	631.61(6)	2248.4(3)	391.04(1)
<i>Z</i>	2	2	8	2
$\rho_{\text{calcd}}$ [g cm <sup>-3</sup> ]	1.964	2.334	2.109	1.326
<i>F</i> (000)	348	420	1392	164
$\mu$ [mm <sup>-1</sup> ]	1.526	7.354	1.635	0.081
index range ( <i>h,k,l</i> )	± 10, ± 9, ± 11	± 10, ± 10, ± 12	± 15, ± 13, ± 20	± 6, ± 7, ± 13
reflins collected	8232	3975	15171	5555
independent reflins/ <i>R</i> <sub>int</sub>	2121/0.029	2546/0.036	1984/0.048	712/0.031
observed reflins [ <i>I</i> > 2 $\sigma$ <i>I</i> ]	1938	2399	1857	668
refined parameters	186	186	178	72
<i>R</i> 1 [observed/all data]	0.0242/0.0276	0.0300/0.0320	0.0184/0.0200	0.0298/0.0315
<i>wR</i> 2 [observed/all data]	0.0694/0.0741	0.0827/0.0839	0.0490/0.0497	0.0779/0.0793
GOF	1.064	1.131	1.076	1.053
$\Delta\rho_{\text{max/min}}$ [e Å <sup>-3</sup> ]	+ 0.61/− 0.81	+ 0.64/− 1.02	+ 0.33/− 0.45	+ 0.15/− 0.15

of 360 s per image (rotation scan modus from  $\phi = 0^\circ$  to  $360^\circ$  with  $\Delta\phi = 2.5^\circ$ ). A total number of 8232 reflections were collected. Decay and absorption effects were corrected with the DECAY algorithm.<sup>[30c]</sup> After merging a sum of 2121 independent reflections remained and were used for all calculations. All non-hydrogen atoms of the molybdenum complex were refined anisotropically. All hydrogen atoms were found in the difference Fourier map and refined with individual isotropic thermal displacement parameters.

**Data collection and refinement for complex 2:** Data collection were performed within the  $\theta$  range of  $2.05^\circ < \theta < 26.34^\circ$  with an exposure time of 90 s per image (3 sets, 344 images,  $\Delta\phi/\Delta\Omega = 1.0^\circ$ ). A total number of 4252 reflections were integrated. Decay and absorption effects were corrected during the scaling procedure.<sup>[30b]</sup> After merging a sum of 2546 independent reflections remained and were used for all calculations. All non-hydrogen atoms of the molybdenum complex were refined anisotropically. All hydrogen atoms were found in the difference Fourier map and refined with individual isotropic thermal displacement parameters.

**Data collection and refinement for complex 4:** Data collection were performed over the  $\theta$  range  $2.51 < \theta < 25.65^\circ$  with an exposure time of 120 s per image (rotation scan modus from  $\phi = 0^\circ$  to  $240^\circ$  with  $\Delta\phi = 1.5^\circ$ ). A total number of 15536 reflections were collected; 364 systematic absent reflections were rejected from the original data set. Decay and absorption effects were corrected with the DECAY algorithm.<sup>[30c]</sup> After merging, a sum of 1984 independent reflections remained and were used for all calculations. All non-hydrogen atoms of the molybdenum complex were refined anisotropically. All hydrogen atoms were found in the difference Fourier map and refined with individual isotropic thermal displacement parameters.

**Data collection and refinement for bipy:** Data collection was performed over the  $\theta$  range  $3.52 < \theta < 25.34^\circ$  with an exposure time of 20 s per image (6 sets, 334 images,  $\Delta\phi/\Delta\Omega = 2.0^\circ$ ). A total number of 5555 reflections were integrated, and 75 systematic absent reflections were rejected from the original data set. Decay and absorption effects were not corrected. After merging, a sum of 712 independent reflections remained and were used for all calculations. All non-hydrogen atoms of the molybdenum complex were refined anisotropically. All hydrogen atoms were found in the difference Fourier map and refined with individual isotropic thermal displacement parameters.

CCDC-177723 (1), CCDC-177721 (2), CCDC-177722 (4), and CCDC-177724 (bipy) contain the supplementary crystallographic data for this paper. These data can be obtained free of charge via [www.ccdc.cam.ac.uk/conts/retrieving.html](http://www.ccdc.cam.ac.uk/conts/retrieving.html) (or from the Cambridge Crystallographic Data Centre, 12 Union Road, Cambridge CB21EZ, UK; fax: (+44) 1223-336-033; or e-mail: [deposit@ccdc.cam.ac.uk](mailto:deposit@ccdc.cam.ac.uk)).

**DFT calculations:** Density functional calculations<sup>[20]</sup> were partially carried out with the Amsterdam Density Functional (ADF) program<sup>[21]</sup> developed by Baerends and co-workers (release 2.3).<sup>[31]</sup> Vosko, Wilk, and Nusair's local exchange correlation potential was used,<sup>[32]</sup> with Becke's nonlocal exchange,<sup>[33]</sup> and Perdew's correlation corrections.<sup>[34]</sup> The geometry optimization procedure was based on the method developed by Versluis and Ziegler,<sup>[35]</sup> with the nonlocal correction terms in the calculation of the gradients. The structure of [MoO<sub>2</sub>Br<sub>2</sub>(2,2'-bipyridine)], BYRPMO, was used to prepare the inputs for the full optimization of the geometry of the complexes. In all the calculations, a triple- $\zeta$  Slater-type orbital (STO) basis set was used for Mo 4s, 5s, 4p, 5p, 4d; double- $\zeta$  STO augmented with a 3d single- $\zeta$  polarization function were used for Br 4s and 4p, C 2s and 2p, N 2s and 2p, O 2s and 2p, and H 1s (basis set I). In a first set of calculations, triple- $\zeta$  STO augmented with a 3d single- $\zeta$  polarization function were used for C 2s and 2p, N 2s and 2p, O 2s and 2p, and H 1s (basis set II). A frozen-core approximation was used to treat the core electrons of Br ([1–3]s, [1–3]p, 3d), C (1s), N (1s), O (1s), and Mo ([1–3]s, [1–3]p, 3d).

DFT calculations with GAUSSIAN98<sup>[25]</sup> were also performed for frequency calculations and geometry optimizations, with the B3LYP functional. This functional includes a mixture of Hartree–Fock exchange with DFT<sup>[20]</sup> exchange-correlation, with the Lee, Yang, and Parr correlation functional, which includes both local and nonlocal terms.<sup>[36]</sup> The 3–21G and 3–21G(\*) basis sets were used for Mo, C, N, O, H, and for X = Br, Cl, CH<sub>3</sub>.<sup>[37]</sup> As the geometries obtained with the 3–21G(\*) basis set showed a better agreement with the experimental structural parameters, as expected, only the results obtained with it are given.

To determine the transition state for the reaction of coordination of an alkyl peroxide to molybdenum, a model complex was considered, where bipyridine was replaced by diazabutadiene. The transition state determination was repeated with the B3LYP method and the 3.21G(\*) basis set, without any symmetry constraints. Transition state structures were searched by means of an eigenvalue-following (mode walking) optimization method.<sup>[38]</sup> The exact nature of the transition state was confirmed by

the frequency analysis, which showed the existence of just one imaginary frequency. The reaction pathways were traced by the intrinsic reaction coordinate (IRC) method.<sup>[39]</sup>

### Acknowledgement

This work was supported by PRAXIS XXI, Project (2/2.1/QUI/419/94). The authors want to thank the DAAD and CRUP (INIDA and Acções Integradas Program) for continuous financial support. ADL, AMS, and AP thank PRAXIS XXI, MG and ESB thank the Alexander von Humboldt foundation for fellowships, and AMS and ISG acknowledge the Bayerische Forschungsstiftung for fellowships. FEK thanks the Fonds der chemischen Industrie for financial support. Prof. J. Mink is acknowledged for helpful discussions and Prof. W. A. Herrmann for continuous support of our work.

- [1] a) S. B. Kumar, M. Chaudhury, *J. Chem. Soc. Dalton Trans.* **1991**, 2169; b) P. Palanca, T. Picher, V. Sanz, P. Gómez-Romero, E. Llopis, A. Domenech, A. Cervilla, *J. Chem. Soc. Chem. Commun.* **1990**, 531; c) J. P. Wilshire, L. Leon, P. Bosserman, D. T. Sawyer, *J. Am. Chem. Soc.* **1979**, *101*, 3379; d) J. M. Berg, R. H. Holm, *J. Am. Chem. Soc.* **1985**, *107*, 925; e) J. P. Caradonna, E. W. Harlan, R. H. Holm, *J. Am. Chem. Soc.* **1986**, *108*, 7856; f) F. J. Feher, K. Rahimian, T. A. Budzichowski, J. W. Ziller, *Organometallics* **1995**, *14*, 3920; g) R. Clarke, M. Gahagan, R. K. Mackie, D. F. Foster, D. J. Cole-Hamilton, M. Nicol, A. W. Montford, *J. Chem. Soc. Dalton Trans.* **1995**, 1221; h) J. R. Backhouse, H. M. Lowe, E. Sinn, S. Suzuki, S. Woodward, *J. Chem. Soc. Dalton Trans.* **1995**, 1489; i) U. Piarulli, D. N. Williams, C. Floriani, G. Gervasio, D. Viterbo, *J. Chem. Soc. Dalton Trans.* **1995**, 3329.
- [2] a) A. F. Hollemann, E. Wiberg, *Lehrbuch der Anorganischen Chemie*, de Gruyter, Berlin, New York, **1995**; b) H. L. Krauss, W. Huber, *Chem. Ber.* **1961**, *94*, 183; c) R. H. Fenn, *J. Chem. Soc. A* **1969**, 1764; d) C. G. Hull, M. B. H. Stiddart, *J. Chem. Soc. A* **1966**, 1633; e) G. Barea, A. Lledos, F. Maseras, Y. Jean, *Inorg. Chem.* **1998**, *37*, 3321; f) M. N. Sheng, G. J. Zajaczk, ARCO, GB 1.136.923, **1968**; g) J. Kollar, Halcon, US 3.350.422, US 3.351.635, **1967**; h) H. Mimoun, I. Seree de Roch, L. Sajus, *Tetrahedron* **1970**, *26*, 37; i) K. B. Sharpless, J. M. Townsend, *J. Am. Chem. Soc.* **1972**, *94*, 295; j) I. V. Yudanov, C. Di Valentin, P. Gisdakis, N. Rösch, *J. Mol. Catal.* **2000**, *158*, 189, and references cited therein; k) J. M. Mitchell, N. S. Finney, *J. Am. Chem. Soc.* **2001**, *123*, 862; l) R. A. Sheldon in *Applied Homogeneous Catalysis with Organometallic Compounds, Vol. 1* (Eds: B. Cornils, W. A. Herrmann), VCH, Weinheim, New York, **1996**; m) F. E. Kühn, W. A. Herrmann *Chemtracts: Org. Chem.* **2001**, *14*, 59; n) G. Wahl, D. Kleinhenz, A. Schorn, J. Sundermeyer, R. Stohwasser, C. Rummey, G. Bringmann, C. Fickert, W. Kiefer, *Chem. Eur. J.* **1999**, *5*, 3237; o) P. Chaumette, H. Mimoun, L. Saussine, J. Fischer, A. Mitschler, *J. Organomet. Chem.* **1983**, *250*, 291; p) R. A. Sheldon in *Aspects of Homogeneous Catalysis, Vol. 4*, pp. 3–70 (Ed: R. Ugo), Reidel, Dordrecht, **1981**.
- [3] a) F. E. Kühn, E. Herdtweck, J. J. Haider, W. A. Herrmann, I. S. Gonçalves, A. D. Lopes, C. C. Romão, *J. Organomet. Chem.* **1999**, 583, 3; b) F. E. Kühn, A. D. Lopes, A. M. Santos, E. Herdtweck, J. J. Haider, C. C. Romão, A. G. Santos, *J. Mol. Catal. A: Chem.* **2000**, *151*, 147; c) A. D. Lopes, Ph. D. Thesis, ITQB/Universidade Nova de Lisboa, **1999**; d) F. E. Kühn, A. M. Santos, A. D. Lopes, I. S. Gonçalves, E. Herdtweck, C. C. Romão, *J. Mol. Catal. A: Chem.* **2000**, *164*, 25; e) F. E. Kühn, A. M. Santos, I. S. Gonçalves, C. C. Romão, A. D. Lopes, *Appl. Organomet. Chem.* **2001**, *15*, 43; f) F. E. Kühn, A. M. Santos, A. D. Lopes, I. S. Gonçalves, J. E. Rodríguez-Borges, M. Pillinger, C. C. Romão, *J. Organomet. Chem.* **2001**, *621*, 207; g) A. M. Santos, F. E. Kühn, K. Bruus-Jensen, I. Lucas, C. C. Romão, E. Herdtweck, *J. Chem. Soc. Dalton Trans.* **2001**, 1332; h) I. S. Gonçalves, C. C. Romão, A. M. Santos, A. D. Lopes, J. E. Rodríguez-Borges, M. Pillinger, P. Ferreira, F. E. Kühn, J. Rocha, *J. Organomet. Chem.* **2001**, *626*, 1; i) M. Groarke, W. A. Herrmann, I. S. Gonçalves, F. E. Kühn, *J. Organomet. Chem.*, in press.
- [4] a) G. N. Schrauzer, L. A. Hughes, N. Strampach, P. R. Robinson, E. O. Schlemper, *Organometallics* **1982**, *1*, 44; b) G. N. Schrauzer, E. O. Schlemper, N. H. Liu, Q. Wang, K. Rubin, X. Zhang, X. Long, C. S. Chin, *Organometallics* **1986**, *5*, 2452; c) G. N. Schrauzer, L. A. Hughes, N. Strampach, F. Ross, D. Ross, E. O. Schlemper, *Organometallics* **1983**, *2*, 481; d) G. N. Schrauzer, L. A. Hughes, E. O. Schlemper, F. Ross, D. Ross, *Organometallics* **1983**, *2*, 1163.
- [5] H. Teruel, A. Sierralta, *J. Mol. Catal. A* **1996**, *107*, 379.
- [6] R. H. Fenn, *J. Chem. Soc. A* **1969**, 1764.
- [7] a) 3D Search and research with the Cambridge Structural Database: F. H. Allen, O. Kennard, *Chem. Des. Automat. News* **1993**, *8*, 1; F. H. Allen, O. Kennard, *Chem. Des. Automat. News* **1993**, *8*, 31; 224400 entries, search for [M(⋯O)2(⋯N)2(⋯AA)2]; b) Search for [M(=O)2(⋯N)2(⋯AA)2]. The refcodes are as follows: BEKNEK, CACWIM, CALSIR, HAGDUO, LETQIK, LETQOQ, MAKYOM, NIPGAU, NIVPOX, PHNOMO, VAFYOQ, VAGDEM, VAGDIQ (2x), VESHUW (2x), VITYIG, VOCTAI, YOMXED, ZEYYIL; c) Search for [M(=O)2(⋯N)2(⋯AA)2]; d) W. Kraus, G. Nolze, *J. Appl. Crystallogr.* **1996**, *29*, 301.
- [8] A. Neves, M. Hörner, H. Fenner, J. Strähle, *Acta Crystallogr. Sect. C* **1993**, *49*, 1737.
- [9] Y.-L. Wong, Y. Yan, E. S. H. Chan, Q. Yang, T. C. W. Mak, D. K. P. Ng, *J. Chem. Soc. Dalton Trans.* **1998**, 3057.
- [10] F. E. Kühn, J. J. Haider, E. Herdtweck, W. A. Herrmann, A. D. Lopes, M. Pillinger, C. C. Romão, *Inorg. Chim. Acta* **1998**, *279*, 44.
- [11] J. B. Parisew, E. M. McCarron, III, R. von Dreele, J. A. Goldstone, *J. Solid State Chem.* **1991**, *93*, 193, and references cited therein.
- [12] *Structure Reports, Vol. 10* (Ed.: A. J. C. Wilson), IUCr, Utrecht, **1946**, p. 110.
- [13] A. Magnéli, *Acta Chem. Scand.* **1957**, *11*, 28.
- [14] G.-P. Charbonneau, Y. Delugeard, *Acta Crystallogr. Sect. B* **1977**, *49*, 1586.
- [15] M. H. Chisholm, J. C. Huffman, I. P. Rothwell, P. G. Bradley, N. Kress, W. H. Woodruff, *J. Am. Chem. Soc.* **1981**, *103*, 4945.
- [16] L. Fernholt, C. Romming, S. Samdal, *Acta Chem. Scand. Ser. A* **1981**, *35*, 707.
- [17] C. C. Romão, F. E. Kühn, W. A. Herrmann, *Chem. Rev.* **1997**, *97*, 3197.
- [18] a) F. E. Kühn, W. A. Herrmann, *Struct. Bonding* **2000**, *97*, 211; b) W. A. Herrmann, R. W. Fischer, D. Marz, *Angew. Chem.* **1991**, *103*, 1706; *Angew. Chem. Int. Ed. Engl.* **1991**, *30*, 1638; c) S. Yamazaki, J. H. Espenson, P. Huston, *Inorg. Chem.* **1993**, *32*, 4683; d) W. A. Herrmann, R. W. Fischer, M. U. Rauch, W. Scherer, *J. Mol. Catal.* **1994**, *86*, 243; e) M. A. Al-Ajlouni, J. H. Espenson, *J. Am. Chem. Soc.* **1995**, *117*, 9243; f) J. Rudolph, K. L. Redding, J. P. Chiang, K. B. Sharpless, *J. Am. Chem. Soc.* **1997**, *119*, 6189; A. K. Yudin, K. B. Sharpless, *J. Am. Chem. Soc.* **1997**, *119*, 11536; g) F. E. Kühn, A. M. Santos, P. W. Roesky, E. Herdtweck, W. Scherer, P. Gisdakis, I. V. Yudanov, C. Di Valentin, N. Rösch, *Chem. Eur. J.* **1999**, 3603.
- [19] a) W. A. Herrmann, F. E. Kühn, M. U. Rauch, J. D. G. Correia, G. Artus, *Inorg. Chem.* **1995**, *34*, 2914; b) M. S. Reynolds, A. Butler, *Inorg. Chem.* **1996**, *35*, 2378, and references therein; c) H. Mimoun, P. Chaumette, M. Mignard, L. Saussine, J. Fischer, R. Weiss, *Nouv. J. Chem.* **1983**, *7*, 467; d) W. P. Griffith, T. D. Wickins, *J. Chem. Soc. A* **1968**, 397.
- [20] a) R. G. Parr, W. Yang, *Density Functional Theory of Atoms and Molecules*, Oxford University Press, New York, **1989**; b) T. Ziegler, *Chem. Rev.* **1991**, *651*, 91.
- [21] Amsterdam Density Functional (ADF) program, release 2.3, Vrije Universiteit: Amsterdam (The Netherlands), **1995**.
- [22] a) K. A. Jørgensen, R. Hoffmann, *Acta Chem. Scand. B* **1986**, *40*, 411; b) W. R. Thiel, *Chem. Ber.* **1996**, *129*, 575; c) K. A. Jørgensen, R. Hoffmann, *J. Am. Chem. Soc.* **1986**, *108*, 1867; d) K. A. Jørgensen, R. A. Wheeler, R. Hoffmann, *J. Am. Chem. Soc.* **1987**, *109*, 3240.
- [23] a) R. D. Bach, G. J. Wolber, B. A. Coddens, *J. Am. Chem. Soc.* **1984**, *106*, 6098; b) Y.-D. Wu, D. K. W. Lai, *J. Org. Chem.* **1995**, *60*, 673; c) A. Hroch, G. Gemmecker, W. R. Thiel, *Eur. J. Inorg. Chem.* **2000**, 1107; d) S. Köstlmeier, O. D. Häberlein, N. Rösch, W. A. Herrmann, *Organometallics* **1996**, *15*, 1872; e) S. Köstlmeier, V. A. Nasluzov, W. A. Herrmann, N. Rösch, *Organometallics* **1997**, *16*, 1786; f) I. V. Yudanov, P. Gisdakis, C. Di Valentin, N. Rösch, *Eur. J. Inorg. Chem.* **1999**, 2135; P. Fantucci, S. Lolli, M. Pizzotti, R. Ugo, *Inorg. Chim. Acta* **1998**, *270*, 479; h) G. Wahl, D. Kleinhenz, A. Schorn, J. Sundermeyer, R. Stowasser, C. Rummey, G. Bringmann, C. Fickert, W. Kiefer, *Chem. Eur. J.* **1999**, *5*, 3237; i) A. Veldkamp, G. Frenking, *J. Am. Chem. Soc.*

- 1994**, 116, 4937; j) D. Tantanak, M. A. Vincent, I. A. Hillier, *Chem. Commun.* **1998**, 1031; k) M. A. Pietsch, T. V. Russo, R. B. Murphy, R. L. Martin, A. K. Rappé, *Organometallics* **1998**, 17, 2716; l) A. K. Rappé, W. A. Goddard, III, *J. Am. Chem. Soc.* **1980**, 102, 5115; m) M. Torrent, L. Deng, M. Duran, M. Sola, T. Ziegler, *Organometallics* **1997**, 16, 13; n) L. Deng, T. Ziegler, *Organometallics* **1997**, 16, 716; o) K. Monteyne, T. Ziegler, *Organometallics* **1998**, 17, 5901.
- [24] a) D. M. P. Mingos, *J. Organomet. Chem.* **1979**, 179, C29; b) K. Tatsumi, R. Hoffmann, *Inorg. Chem.* **1980**, 19, 2656; c) D. C. Brower, J. L. Templeton, D. M. P. Mingos, *J. Am. Chem. Soc.* **1987**, 109, 5203; d) I. Demachy, Y. Jean, *Inorg. Chem.* **1996**, 35, 5027.
- [25] Gaussian98, Revision A7, M. J. Frisch, G. W. Trucks, H. B. Schlegel, G. E. Scuseria, M. A. Robb, J. R. Cheeseman, V. G. Zakrzewski, J. A. Montgomery, Jr., R. E. Stratmann, J. C. Burant, S. Dapprich, J. M. Millam, A. D. Daniels, K. N. Kudin, M. C. Strain, O. Farkas, J. Tomasi, V. Barone, M. Cossi, R. Cammi, B. Mennucci, C. Pomelli, C. Adamo, S. Clifford, J. Ochterski, G. A. Petersson, P. Y. Ayala, Q. Cui, K. Morokuma, D. K. Malick, A. D. Rabuck, K. Raghavachari, J. B. Foresman, J. Cioslowski, J. V. Ortiz, A. G. Baboul, B. B. Stefanov, G. Liu, A. Liashenko, P. Piskorz, I. Komaromi, R. Gomperts, R. L. Martin, D. J. Fox, T. Keith, M. A. Al-Laham, C. Y. Peng, A. Nanayakkara, C. Gonzalez, M. Challacombe, P. M. W. Gill, B. Johnson, W. Chen, M. W. Wong, J. L. Andres, C. Gonzalez, M. Head-Gordon, E. S. Replogle, J. A. Pople, Gaussian, Inc., Pittsburgh PA, **1998**.
- [26] R. Colton, I. B. Tomkins, *Aust. J. Chem.* **1965**, 18, 447.
- [27] G. N. Schrauzer, E. L. Moorehead, J. H. Grate, L. Hughes, *J. Am. Chem. Soc.* **1978**, 100, 4760.
- [28] W. M. Carmichael, D. A. Edotch, G. W. A. Fowlor, B. R. Marchel, *Inorg. Chim. Acta* **1967**, 1, 93.
- [29] a) P. Chaumette, H. Mimoun, L. Saussine, J. Fischer, A. Mitschler, *J. Organomet. Chem.* **1983**, 250, 291; b) E. P. Talsi, O. V. Klimov, K. I. Zamaraev, *J. Mol. Catal.* **1993**, 83, 329; c) E. P. Talsi, K. V. Shalyaev, K. I. Zamaraev, *J. Mol. Catal.* **1993**, 83, 347.
- [30] Data collection and data reduction: a) Nonius MACH3 Operating System Version 5.1, Nonius B. V., Delft (The Netherlands), **1994**; b) IPDS Operating System Version 2.8., Stoe&Cie. GmbH, Darmstadt (Germany), **1999**; c) Z. Otwinowski, W. Minor, *Methods Enzymol.* **1997**, 276, 307; Structure solution and refinement: d) A. Altomare, G. Cascarano, C. Giacovazzo, A. Guagliardi, M. C. Burla, G. Polidori, M. Camalli, *Sir92, J. Appl. Crystallogr.* **1994**, 27, 435; e) G. M. Sheldrick, SHELXL-97, University of Göttingen, Göttingen (Germany), **1998**; f) *Tables for Crystallography, Vol. C* (Ed.: A. J. C. Wilson), Kluwer Academic Publishers, Dordrecht (The Netherlands), **1992**, Tables 6.1.1.4 (pp. 500–502), 4.2.6.8 (pp. 219–222), and 4.2.4.2 (pp. 193–199); g) G. Artus, W. Scherer, T. Priermeier, E. Herdtweck, Strux-V, A Program System to Handle X-Ray Data, TU München (Germany), **1997**; Graphics: h) A. L. Spek, Platon, A Multipurpose Crystallographic Tool, Utrecht University, Utrecht (The Netherlands), **1999**.
- [31] a) E. J. Baerends, D. Ellis, P. Ros, *Chem. Phys.* **1973**, 2, 41; b) E. J. Baerends, P. Ros, *Int. J. Quantum Chem.* **1978**, S12, 169; c) P. M. Boerrigter, G. te Velde, E. J. Baerends, *Int. J. Quantum Chem.* **1988**, 33, 87; d) G. te Velde, E. J. Baerends, *J. Comp. Phys.* **1992**, 99, 84.
- [32] S. H. Vosko, L. Wilk, M. Nusair, *Can. J. Phys.* **1980**, 58, 1200.
- [33] A. D. Becke, *J. Chem. Phys.* **1987**, 88, 1053.
- [34] a) J. P. Perdew, *Phys. Rev. B* **1986**, 33, 8822; b) J. P. Perdew, *Phys. Rev. B* **1986**, 34, 7406.
- [35] a) L. Versluis, T. Ziegler, *J. Chem. Phys.* **1988**, 88, 322; b) L. Fan, T. Ziegler, *J. Chem. Phys.* **1991**, 95, 7401.
- [36] a) C. Lee, W. Yang, R. G. Parr, *Phys. Rev. B* **1988**, 37, 785; b) A. Becke, *J. Chem. Phys.* **1993**, 98, 5648; c) P. J. Stephens, F. J. Delvin, C. F. Chabalowsky, M. J. Frisch, *J. Phys. Chem.* **1994**, 98, 11623.
- [37] a) J. S. Binkley, J. A. Pople, W. J. Hehre, *J. Am. Chem. Soc.* **1980**, 102, 939; b) M. S. Binkley, J. A. Pople, W. J. Pietro, W. J. Hehre, *J. Am. Chem. Soc.* **1982**, 104, 2797; c) W. J. Pietro, M. Francl, W. J. Hehre, D. J. Defrees, J. A. Pople, J. S. Binkley, *J. Am. Chem. Soc.* **1982**, 104, 5039; d) K. Dobbs, W. J. Hehre, *J. Comput. Chem.* **1986**, 7, 359; e) K. Dobbs, W. J. Hehre, *J. Comput. Chem.* **1987**, 8, 861; f) K. Dobbs, W. J. Hehre, *J. Comput. Chem.* **1987**, 8, 880.
- [38] a) J. Baker, *J. Comp. Chem.* **1986**, 7, 385; b) J. Baker, *J. Comp. Chem.* **1987**, 8, 563; c) H. B. Schlegel in *New Theoretical Concepts for Understanding Organic Reactions* (Ed.: J. Bertran), Kluwer Academic (The Netherlands), **1989**, p. 33.
- [39] a) C. Gonzalez, H. B. Schlegel, *J. Chem. Phys.* **1989**, 90, 2154; b) C. Gonzalez, H. B. Schlegel, *J. Phys. Chem.* **1990**, 94, 5523.

Received: July 20, 2001

Revised: December 12, 2001 [F3429]